THE JOURNAL OF COMPARATIVE NEUROLOGY 379:150–170 (1997)

Cell-Type Specific Organization of Glycine Receptor Clusters in the Mammalian Spinal Cord

FRANCISCO J. ALVAREZ,* DIANNE E. DEWEY, DEBORAH A. HARRINGTON, AND ROBERT E.W. FYFFE
Department of Anatomy, Wright State University, Dayton, Ohio 45435

ABSTRACT

Glycinergic synapses play a major role in shaping the activity of spinal cord neurons. The spatial organization of postsynaptic receptors is likely to determine many functional parameters at these synapses and is probably related to the integrative capabilities of different neurons. In the present study, we have investigated the organization of gephyrin expression along the dendritic membranes of α- and γ-motoneurons, Ia inhibitory interneurons, and Renshaw cells. Gephyrin is a protein responsible for the postsynaptic clustering of glycine receptors, and the features of gephyrin and glycine receptor α_1-subunit immunofluorescent clusters displayed similar characteristics on ventral horn spinal neurons. However, the density of clusters and their topographical organization and architecture varied widely in different neurons and in different dendritic regions. For motoneurons and Ia inhibitory interneurons, cluster size and complexity increased with distance from the soma, perhaps as a mechanism to enhance the influence of distal synapses. Renshaw cells were special in that they displayed an abundant complement of large and morphologically complex clusters concentrated in their somas and proximal dendrites. Serial electron microscopy confirmed that the various immunoreactivity patterns observed with immunofluorescence accurately parallel the variable organization of pre- and postsynaptic active zones of glycinergic synapses. Finally, synaptic boutons from single-labeled axons of glycinergic neurons (Ia inhibitory interneurons) were also associated with postsynaptic receptor clusters of variable shapes and configurations. Our results indicate that mechanisms regulating receptor clustering do so primarily in the context of the postsynaptic neuron identity and localization in the dendritic arbor. J. Comp. Neurol. 379:150–170, 1997.

Indexing terms: gephyrin; motoneurons; Ia inhibitory interneurons; Renshaw cells; synaptic active zones

The specific integrative properties of central neurons depend largely on the organized distribution of synapses and neurotransmitter receptors along their dendritic arbors (Rall et al., 1992; Spruston et al., 1994). Indeed, the structural organization of postsynaptic densities (containing the postsynaptic receptor clusters) has been proposed as a major factor in determining the functional characteristics of individual synapses in the hippocampus (Lisman and Harris, 1993; Edwards, 1995). In the present study, we have investigated the architecture and densities of glycine receptor clusters in different types and membrane compartments (e.g., proximal vs. distal dendrites) of ventral horn spinal cord neurons. Much recent research has focused on the fine immunocytochemical localization of neurotransmitter receptors. However, for most central neurons, receptor immunolocalization has been described only for the cell soma and the most proximal dendritic regions. Furthermore, systematic analysis of receptor organization in defined interneurons has been especially hindered by the fact that their cell bodies and dendritic arborizations cannot usually be positively identified in most immunocytochemical studies without using additional means to verify their identity and to label them specifically. Finally, except for a previous report on the large specialized dendrites of the teleost Mauthner cell (Triller et al., 1990), the differential organization of immunoreactive receptor clusters at distal vs. proximal synapses on the highly branched dendritic trees of central neurons has not been addressed before.

Contract grant sponsor: NIH-NINDS; Contract grant numbers: NS25547, NS33555.

*Correspondence to: Francisco J. Alvarez, Ph.D., Department of Anatomy, Wright State University, 3640 Col. Glenn Hwy., Dayton, OH 45435.
E-mail: FALVAREZ@desire.wright.edu

Received 15 April 1996; Revised 2 August 1996; Accepted 29 August 1996

In the present study, we have used a combination of electrophysiological identification, intracellular staining, and immunocytochemical localization to examine the principles governing the organization of glycine receptor clusters throughout the whole somatodendritic membrane of two types of interneurons [Renshaw cells (RCs) and Ia inhibitory interneurons (IaINs)] and α- and γ-motoneurons (αMNs, γMNs). These neurons constitute well known elements of the spinal segmental motor network and greatly differ in their physiology, structure, and synaptology (reviewed in Baldissera et al., 1981; Windhorst, 1990; Jankowska, 1992). Briefly, RCs and IaINs are two major inhibitory interneurons that shape MN firing through recurrent (Renshaw 1941; Eccles et al., 1954) and reciprocal inhibitory circuits, respectively (Eccles et al., 1956). Both interneurons exert synaptic actions on MNs through glycinergic mechanisms and are themselves subject to potent inhibitory glycinergic control (Eccles et al., 1954; Curtis et al., 1968; recent reviews in Schneider and Fyffe, 1992; Jankowska, 1992).

Synaptically released glycine exerts its effects by activating postsynaptic ligand-gated chloride channels comprising ligand-binding (α-) and structural (β-) subunits (reviewed in Betz, 1992). In addition, a 93 kDa peripheral cytoplasmic membrane protein, named gephyrin, was found to be intimately associated with the α-and β-transmembrane subunits (Pfeiffer et al., 1982; Schmitt et al., 1987). Gephyrin probably directs the anchoring of glycine receptor clusters in the postsynaptic plasma membrane while contributing also to the mature biophysical properties of the receptor (Kirsch et al., 1991, 1993; Takagi et al., 1992; Kirsch and Betz, 1995; Meyer et al., 1995). Antibodies against gephyrin have been used extensively to immunolocalize postsynaptic glycine receptors clusters in many different brain regions. Some observations suggested that in some cases the distribution of gephyrin immunoreactivity could be more extensive than that of transmembrane α-subunits of the glycine receptor and could be associated with other membrane protein complexes that include glycine receptor β-subunits in their structure (Kirsch and Betz, 1993). In this study, we validate the use of gephyrin immunoreactivity as a marker of postsynaptic glycine receptor clusters in the spinal cord ventral horn and use it to analyze the location and structural organization of glycine receptor clusters in the dendritic arbors of four different neuronal types. Preliminary results have been published as abstracts (Alvarez et al., 1993; Fyffe et al., 1993), and a preliminary account of motoneuron gephyrin clustering has appeared in a volume of a symposium proceedings (Fyffe et al., 1995).

MATERIALS AND METHODS

Double immunofluorescence for gephyrin and glycine receptor α-subunits

Adult cats (n = 3) were euthanized with an overdose of Nembutal (~200 mg i.v.) and perfused via the left ventricle with cold phosphate-buffered saline (PBS), followed by cold fixative (4% paraformaldehyde in 0.1 M phosphate buffer, pH 7.4). Spinal cord blocks were postfixed for 0–12 hours at 4°C, then stored in phosphate buffer with 15% sucrose until cut. Fifty-micrometer-thick transverse sections were obtained on a vibratome. We observed that more than 15 minutes of postfixation severely diminished immunostaining with antibodies against extracellular epitopes of α-subunits but that gephyrin immunoreactivity was quite resistant to stronger fixation (see also Kirsch and Betz, 1993).

Two methods were employed for dual immunofluorescence. First, an "epitope masking" method was used following Triller et al. (1987); the sections were incubated first with mouse monoclonal antibody (mAb) 2b (diluted 1:10) directed against an extracellular epitope of the glycine receptor α_1-subunit (Pfeiffer et al., 1984; kindly donated by Drs. J. Kirsch and H. Betz, Max-Plank Institute, Frankfurt, Germany). Immunoreactive sites were revealed with a fluorescein isothiocyanate (FITC)-coupled goat anti-mouse IgG (Jackson, West Grove, PA). Then, all mouse IgG antigenic determinants were covered with excess goat anti-mouse antibodies (1:20; Jackson). Afterwards, the sections were blocked again with normal goat serum (1:10) and placed in mouse mAb 7a (against gephyrin; Boehringer Mannheim, Indianapolis, IN; 0.5 μg/ml in PBS/0.1% Triton X-100 at 4°C overnight). The immunoreactive sites were revealed by incubating the sections for 2 hours at room temperature with goat anti-mouse IgG serum coupled to tetramethylrhodamine isothiocyanate (TRITC; Jackson). Controls to detect artifactual colocalization included sections in which the gephyrin antiserum was replaced by PBS or by a similar concentration (0.5 μg/ml) of nonspecific mouse IgGs (Sigma, St. Louis, MO). The second control indicated abundant artifactual colocalization when this method is used (see Results).

A second method, developed by Tramu et al. (1978), based on the elution and/or denaturation of all antibodies, was implemented as described by Larsson (1988). Staining was performed as described above by using mAb 2b, and the immunofluorescence in selected sections was then extensively photographed at high and low magnification. Thereafter, all antibodies were eluted/denatured by incubating the sections twice for 5 minutes in dH_2O, for 10–15 minutes in a solution containing 0.017% $KMnO_4$ and 0.04% H_2SO_4, and for 30 seconds in 0.5% $Na_2S_2O_5$; washing them in running H_2O for 20 minutes; and finally returning them to PBS. Some control sections were then visualized under epifluorescence before and after incubation with goat anti-mouse IgG antiserum coupled to FITC (1:50 Jackson) to assess the complete disappearance of fluorescence and mouse IgG epitopes from the first immunoreaction against α_1-subunits. Finally, a second immunoreaction was performed against gephyrin by using mAb 7a as described above. The regions photographed after the first immunoreaction against α_1-subunits were now analyzed for gephyrin immunoreactivity. This approach demonstrated that gephyrin antibodies are very accurate tools for analyzing the structure of glycine receptor clusters on cat ventral horn cells. Furthermore, the resistance of gephyrin epitopes to strong fixation made mAb 7a more suitable for detailed structural analysis of immunoreactivity on the dendritic arbors of intracellularly filled neurons followed through serial sections (see below).

Combined electrophysiological characterization, intracellular labeling, and gephyrin immunofluorescence

Animal preparation. The experiments were performed on the spinal cords of 14 adult cats and followed previously described methods (Fyffe, 1991a,b). All animals were deeply anesthetized with Nembutal (initially 40 mg/kg i.p., then 5 mg/ml i.v. as required to maintain a deep

level of anesthesia). The study was conducted in compliance with approved institutional animal care and use protocols and according to NIH guidelines. Cannulae were placed in the left carotid artery, for continuous monitoring of blood pressure and heart rate, and in the left external jugular vein, for administration of anesthetics, drugs, and fluids. The trachea was intubated to permit artificial ventilation and continuous measurement of the end-tidal CO_2 level, which was maintained near 4% (~32 mm Hg) by adjustment of the mechanical ventilator. Body temperature was continuously monitored and maintained near 37°C by a homeothermic blanket. The bladder was catheterized for collection of urine (keeping the bladder empty also helped to maximize the stability of the preparation). The cat was fixed rigidly in a Lundberg-type stereotaxic headholder and spinal frame. Peripheral nerves to the medial and lateral gastrocnemius and soleus and posterior biceps and semitendinosus muscle groups were dissected and mounted on Ag/AgCl-stimulating electrodes. The sciatic nerve was also mounted in continuity on stimulating electrodes for antidromic activation of motoneurons. Following a laminectomy to expose spinal segments L_3–S_2, dorsal roots L_6–S_1 were cut and their central ends mounted on stimulating electrodes. Ventral roots were left intact. During the recording period, the cat was paralyzed with gallamine triethiodide (Flaxedil; 20–40 mg i.v.) and maintained in deep anesthesia, as assessed by blood pressure, heart rate, and pupillary constriction.

Microelectrodes for intracellular recording and staining. We used beveled electrodes filled with 4–8% neurobiotin (Vector Laboratories, Burlingame, CA) in 0.1 M Tris/0.5 M KCl, pH 7.6 (electrode resistance 20–35 MΩ). Intracellular recordings and injections were performed as described elsewhere (Fyffe, 1991a,b).

Cell identification. αMNs were identified by the conduction velocity of their antidromic action potential and by the presence of monosynaptic excitatory postsynaptic potentials (epsps) following dorsal root stimulation at a strength sufficient to activate group I fibers. γMNs were identified by antidromic conduction velocity and lack of monosynaptic input from large-diameter dorsal root fibers (Moschovakis et al., 1991). In this study, we considered conduction velocities of less than 40 $msec^{-1}$ to represent γMNs. Renshaw cells were identified by their characteristic high-frequency discharge following motor axon activation (see Fyffe, 1991a). Ia inhibitory interneurons were identified by monosynaptic activation following dorsal root stimulation at group I strength and by recurrent inhibition, but no antidromic activation, following motor axon stimulation (see Fyffe, 1991b). In all cases, the morphology, location, and axonal trajectory of the stained cell were subsequently used to confirm the cell's identity.

Perfusion and tissue processing. After completion of the electrophysiological recordings and intracellular injections, the cats were euthanized with an overdose of Nembutal (~200 mg i.v.) and perfused with 4% paraformaldehyde in 0.1 M phosphate buffer (pH 7.4) as described above. Spinal cord blocks were postfixed for 4–8 hours at 4°C, then stored in phosphate buffer with 15% sucrose until cut. Serial 50-μm-thick sections (transverse or longitudinal) were obtained on a Vibratome.

Visualization of intracellularly stained neurons. Neurobiotin-labeled cells were revealed with 7-amino-4-methylcoumarin-3-acetic acid (AMCA)-labeled avidin (Vector Laboratories; 1:10 dilution in PBS/0.1% Triton X-100; incubation for 2–3 hours at room temperature). Tissue autofluorescence was prevented by preincubating the sections in 1% $NaHB_4$ in PBS (for 30 minutes at room temperature) before the application of the avidin-AMCA marker.

Immunocytochemistry. After several PBS rinses, the sections were blocked with normal goat serum (1:10) and placed in mAb 7a (Boehringer Mannheim; 0.5 μg/ml in PBS/0.1% Triton X-100, at 4°C for 2–3 days). The immunoreactive sites were revealed by incubating the sections for 2 hours at room temperature with a goat anti-mouse IgG serum coupled to FITC (Jackson) diluted 1:50 in PBS/0.1% Triton X-100. Sections were coverslipped with Vectashield antifading medium (Vector Laboratories).

Brightfield visualization of the intracellular marker. Following detailed examination under fluorescence microscopy, the intracellular label was revealed with peroxidase for subsequent computer-aided reconstruction and quantitative morphometric analysis under brightfield illumination. This was accomplished by removing the coverslips and processing the sections (on the slide) with an ABC kit (Vector Laboratories) and visualizing the peroxidase with 0.02 mg/ml diaminobenzidine (DAB; Sigma) and 0.01% H_2O_2 in 0.05 M Tris. The reaction was enhanced by adding 0.01% nickel ammonium sulfate.

Analysis. Sections were analyzed for double immunofluorescence by using an Olympus fluorescence microscope fitted with an ultraviolet (UV) excitation block (Olympus, Lake Success, NY) for visualization of intracellular AMCA (blue fluorescence) and with a blue excitation block (Chroma Tech., Brattleboro, VT) for visualization of the fluorescein immunolabel (green fluorescence). We also used a "triple" filter block (Chroma Tech.) that allows visualization of both markers simultaneously to confirm further the location of gephyrin immunoreactivity inside labeled dendrites. All microphotography of gephyrin-immunoreactive (gephyrin-IR) clusters over identified neurites was performed by using a ×100 oil objective (N.A. 1,30). After extensive fluorescence photography, intracellularly stained neurons were reconstructed in three dimensions by using a computer-aided neuron tracing system (Eutectic NTS; Sun Technologies, Raleigh, NC), which also permitted measurement of dendritic length and membrane surface area. Photographs of gephyrin-IR clusters were precisely correlated with these reconstructions and analyzed according to distance to the cell soma. Density of clusters was assessed qualitatively. Immunoreactive cluster sizes were measured individually in their long axis in photographic pictures obtained at ×100 and enlarged 4–5 times. Under these conditions and taking into account edge and out-of-focus fluorescent haze of immunofluorescent spots contained in 50-μm-thick tissue sections, we estimated our resolution to be approximately 0.5 μm (see also Koulen et al., 1996). To provide the most unbiased representation of cluster sizes, we therefore grouped them in 0.5 μm bins and plotted them according to their locations in the dendritic arbor. Five distance categories were used: 0–100, 100–200, 200–500, 500–1,000, and over 1,000 μm of path length in the dendritic arbor. To determine whether significant differences exist in cluster size by cell type or distance category, we conducted a three-way mixed-effects analysis of variance (ANOVA) of the averages and standard deviations of cluster sizes in each distance category and in each cell type. The three factors (independent variables) in this ANOVA model include

distance category, cell type, and particular cell examined. Two cells of each type were analyzed. In this model, distance and cell type were considered fixed effects, and the particular neuron used was included as a random effect nested within cell type. The effect of cell type by distance category and the effect of distance in each cell were analyzed using two-way mixed-effects ANOVA. Nine different ANOVAS of this kind were performed, one for each of the four cell types and one for each of the five distance categories considered. In analyzing distance categories, the two factors in each ANOVA were cell type and the particular cell sampled; in this way we could account for variability resulting from cell and separate this from variability resulting from cell type. In analyzing each cell type individually, distance and cell analyzed were included in each ANOVA model as factors. The assumptions of ANOVA models were met reasonably well by our data; although there was some departure from normality, this was not enough to warrant using nonparametric techniques. Finally, in order to determine how selected data pairs differ, we conducted Fisher's least significant difference (LSD) multiple comparison procedures when significant differences in the data series were revealed in our ANOVA models. This test allowed us to compare our data with reasonable accuracy even when samples had unequal sizes. In order to determine how clusters sizes differ with distance in individual cell types, we compared each distance category with all the others for each individual cell type and then determined which one was larger once statistical differences were revealed. To compare cluster sizes found at similar locations in different cell types, we used a similar test to compare the average cluster size at a fixed distance in the four cell types. All the statistical analysis was conducted by using SAS version 6.10. Statistical significance was set at $P < 0.01$ for all tests.

Serial section electron microscopic reconstruction of gephyrin-IR clusters in the cat ventral horn

General electron microscopy procedures. Tissue from the lumbosacral spinal cord of two cats was processed for electron microscopy. The animals were perfused as described above, but 0.4% glutaraldehyde was included in the fixative for ultrastructural preservation. No decrease of gephyrin immunoreactivity was observed with electron microscopy in comparison to that found in light microscopy specimens. Sections were obtained on a Vibratome, excess aldehydes were blocked with 1% $NaBH_4$, and the sections were then immunostained by using mAb 7a (dilution 0.5 μg/ml in PBS) and revealed with a mouse ABC Vector kit by using DAB as the final chromogen (0.02% DAB, 0.01% H_2O_2 in 0.05 M Tris). For electron microscopic purposes, we avoided the use of Triton X-100 in all incubations and shortened the primary antibody incubation to 12 hours. After immunocytochemistry, sections were washed in PBS, postfixed in 2% osmium tetroxide, stained en bloc with uranyl acetate, dehydrated in a graded series of alcohols, cleared through two changes of propylene oxide, infiltrated with 1:1 propylene oxide/Epon-Araldite, and finally flat embedded in Epon-Araldite resin between fluorocarbon-coated coverslips. Regions of interest were identified, photographed, and drawn with light microscopy. Small chips containing these regions were cut from the wafer and glued onto a resin EM block. Ultrathin sections were obtained in a Sorvall MT 6000 ultramicrotome. Serial sections were collected on nickel or copper single-slot grids coated with a thin layer of formvar. Some grids were counterstained for several minutes in lead citrate. Sections were viewed on a Philips EM 300 or Philips EM 201 transmission electron microscope at 60 or 80 kV.

Three-dimensional reconstruction of individual synaptic interactions. Serial photographs of selected synaptic boutons impinging on proximal dendrites or cell somas of neurons displaying different gephyrin-IR cluster arrangements were used for 3D reconstruction and morphometric analysis by means of the RECON software of the Eutectic system. Bouton profiles were traced on a digitizing tablet marking the extent of the immunoreactivity, the synapse active zones, and the apposition between the membranes of the pre- and postsynaptic structures. Data from serial electron micrographs (usually enlarged to ×50,000 final magnification) were entered into the Eutectic 3D Reconstruction and Analysis System. Serial electron micrographs were aligned by thresholding and capturing in a video monitor the outlines of various profiles occupying large areas within an electron micrograph and then using these binary image outlines to align on the same monitor the live gray image of the next electron micrograph in the series. 3D reconstructions of synaptic boutons presynaptic to gephyrin-IR spots and 2D projection maps of the active, apposition, and immunoreactive zones were then generated. Two-dimensional projection maps generated in the Eutectic System were scanned (HP ScanJet 4c) and analyzed by using Image Pro Plus imaging software (Media Cybernetics, Silver Spring, MD).

RESULTS

Gephyrin-IR clusters were detected on the dendritic arbors of α- and γ-motoneurons (αMNs, γMNs), Renshaw cells (RCs), and Ia inhibitory interneurons (IaINs) by combining electrophysiological characterization and intracellular labeling of single cells, followed by immunofluorescence labeling. Gephyrin-IR clusters showed considerable morphological variability depending both on their localization in specific neuronal types and on their position in the dendritic arbor. They varied from small punctae (<0.5 μm in diameter) to more complicated structures, including perforated patches, horseshoe figures, scalloped profiles, and combinations of these shapes (sometimes measuring more than 3 μm along their longest axis; e.g., see Fig. 1A,C,E). Smaller patches consistently displayed dimmer (and faster fading) immunofluorescence.

Association of gephyrin with glycine receptors in the ventral horn of the cat spinal cord

Gephyrin-IR clusters faithfully represented the location and morphology of glycine receptor clusters, as demonstrated by using double immunofluorescence (see Materials and Methods). Double immunofluorescence studies using mAb 7a to reveal gephyrin immunoreactivity and mAb 2b to reveal α_1-subunit immunoreactivity were carried out by using an elution/denaturing technique (Tramu et al., 1978; Larsson, 1988) or an "epitope masking" method used previously for the same purpose (Triller et al., 1987). As was reported by Triller et al. (1987), extensive colocalization of 2b and 7a immunoreactivities was observed with the latter method. PBS controls were negative, in agreement with results obtained previously (Triller et

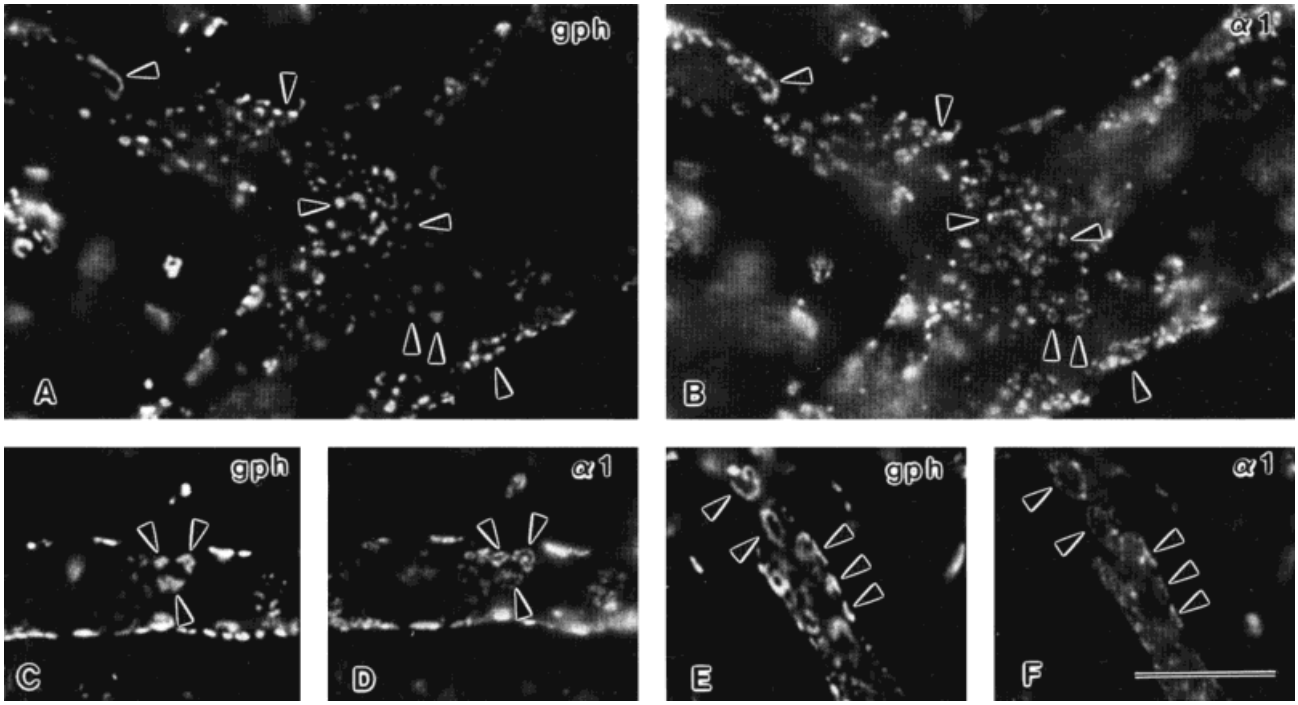

Fig. 1. Colocalization of gephyrin and the α_1-subunit of the glycine receptor in small (A,B), medium-sized (C,D), and large (E,F) receptor patches. **A–F:** Photomicrograph pairs of immunofluorescent gephyrin (gph; A,C,E) and α_1-subunit (α_1; B,D,F) clusters. α_1-Subunits colocalized with gephyrin-IR clusters in a 1:1 relationship over the cell somas and dendrites of ventral horn neurons (see matching arrowheads for each pair of micrographs). Small/simple or large/complex gephyrin-IR clusters parallel similar variations in α_1-subunit immunofluorescence patches. However, α_1-subunit immunofluorescence was frequently found to occupy predominantly the periphery of the gephyrin-IR patch (see, especially, C,D). All micrographs are at the same magnification. Scale bar = 10 μm.

al., 1987), suggesting effective masking of mouse IgG epitopes from mAb 2b to the TRITC-labeled antiserum used in the second immunoreaction. However, considerable TRITC immunolabeling that exactly colocalized with 2b-FITC immunofluorescence was found in sections incubated with random mouse IgGs instead of 7a antibody. This spurious cross-reactivity probably arises from binding of mouse IgGs to the free binding sites of the blocking immunoglobulins (Larsson, 1988). We therefore concluded that this "epitope masking" method was unacceptable for effective assessment of the degree of colocalization of mAb 2b and 7a immunoreactivity (cf. Triller et al., 1987). However, it should be noted that the labeling intensity produced by neutral mouse IgGs was lower than that produced by mAb 7a, indicating that specific staining of gephyrin epitopes also occurred at the same sites.

In contrast, extensive controls at every step of the elution/denaturing method (see Materials and Methods) indicated that there was little or no cross-reactivity between 2b and 7a immunofluorescence when using this technique. However, the strong treatments used to elute or denature antibodies produced significant shrinkage of the tissue, and sometimes groups of immunoreactive clusters identified in consecutive immunoreactions fell in different focal planes or their relative dimensions were slightly distorted. Despite these pitfalls, the results clearly demonstrated that both proteins codistribute exactly to the same patches of membrane in ventral horn neurons and that there is a close equivalence between the morphologies of gephyrin immunoreactivity and the corresponding α_1-subunit-IR patches (Fig. 1). At high magnification, it was also observed that α_1-subunit immunoreactivity was not uniformly dense over the area demarcated by gephyrin immunoreactivity, frequently being more intense in the periphery of the larger gephyrin-IR patches.

Gephyrin immunoreactivity on the soma and dendritic membranes of motoneurons

αMNs (n = 14) displayed gephyrin immunoreactivity throughout their dendritic trees but with different densities at different locations (Figs. 2–4). The presence of glycine receptor clusters associated with labeled dendrites

Fig. 2. Double-fluorescence micrographs of gephyrin-IR clusters on intracellularly labeled motoneuron dendrites. These pictures were obtained using a filter cube that permits simultaneous visualization of the true color fluorescence of AMCA (blue intracellular label) and FITC (green gephyrin immunofluorescence). **A:** Very proximal dendritic segment (less than 100 μm from the cell soma) and its first dendritic branching point displaying a dense surface covering by small, dot-like, gephyrin immunofluorescent clusters. Part of the axon hillock is indicated (ax) originating from the proximal dendritic trunk. **B:** Distal dendritic segment (farther than 850 μm from the cell body) shows larger and more complex gephyrin-immunofluorescent clusters. Complex morphologies and perforations can be best observed in those clusters visualized "en face" (arrowheads). Distally, gephyrin-immunofluorescent clusters also appear more sparsely distributed. **C,D:** Two different segments of middle regions of the same dendrite (300–500 μm from the cell soma) show gephyrin-immunofluorescent aggregates of variable sizes at densities intermediate between proximal (A) and distal (B) locations. In C and D, the focal plane of the micrograph cuts through the middle of the dendrite; hence, a side view of "in focus" gephyrin-immunofluorescent clusters is rendered, preventing full visualization of their structure. All pictures are at the same magnification. Scale bar = 10 μm in D.

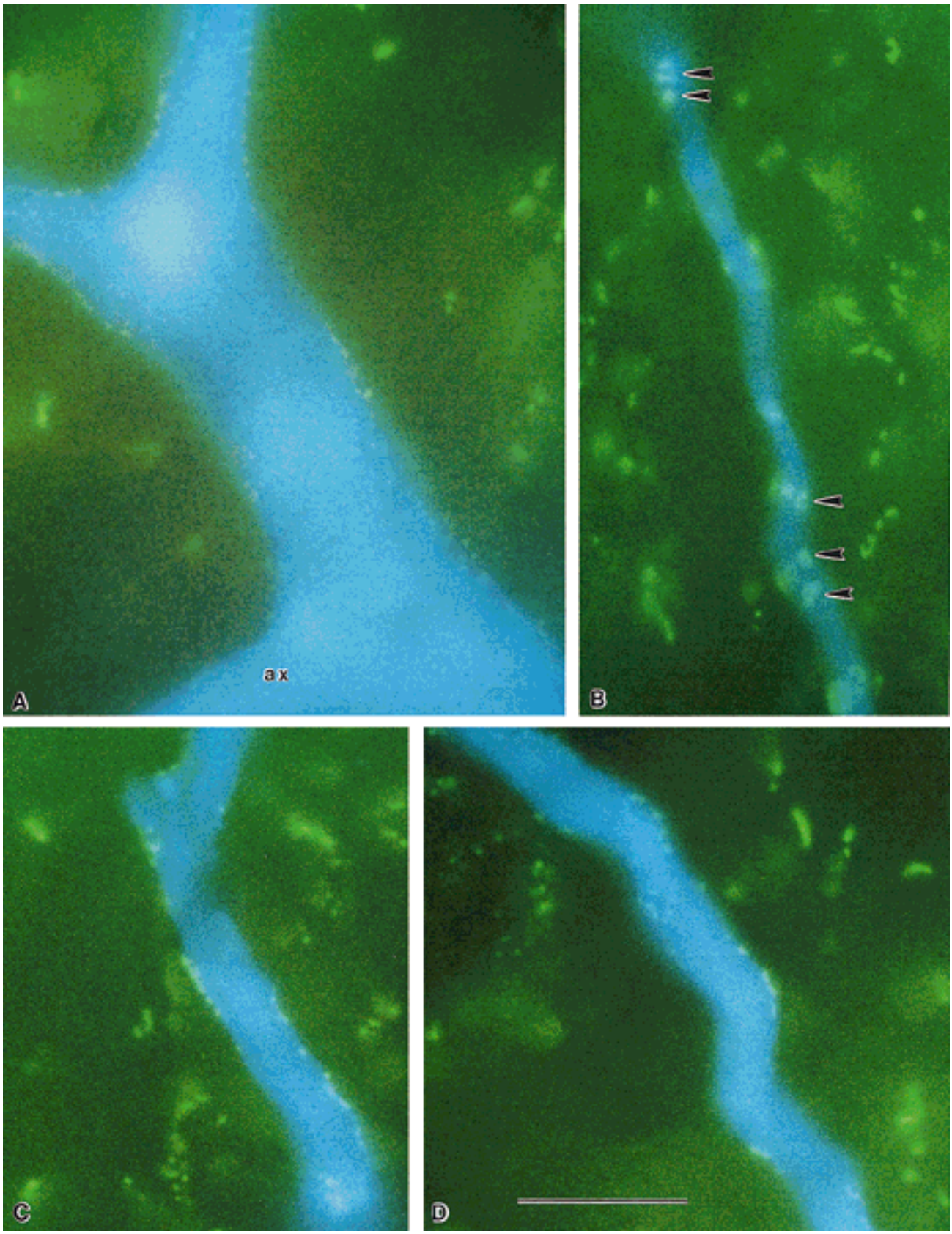

Figure 2

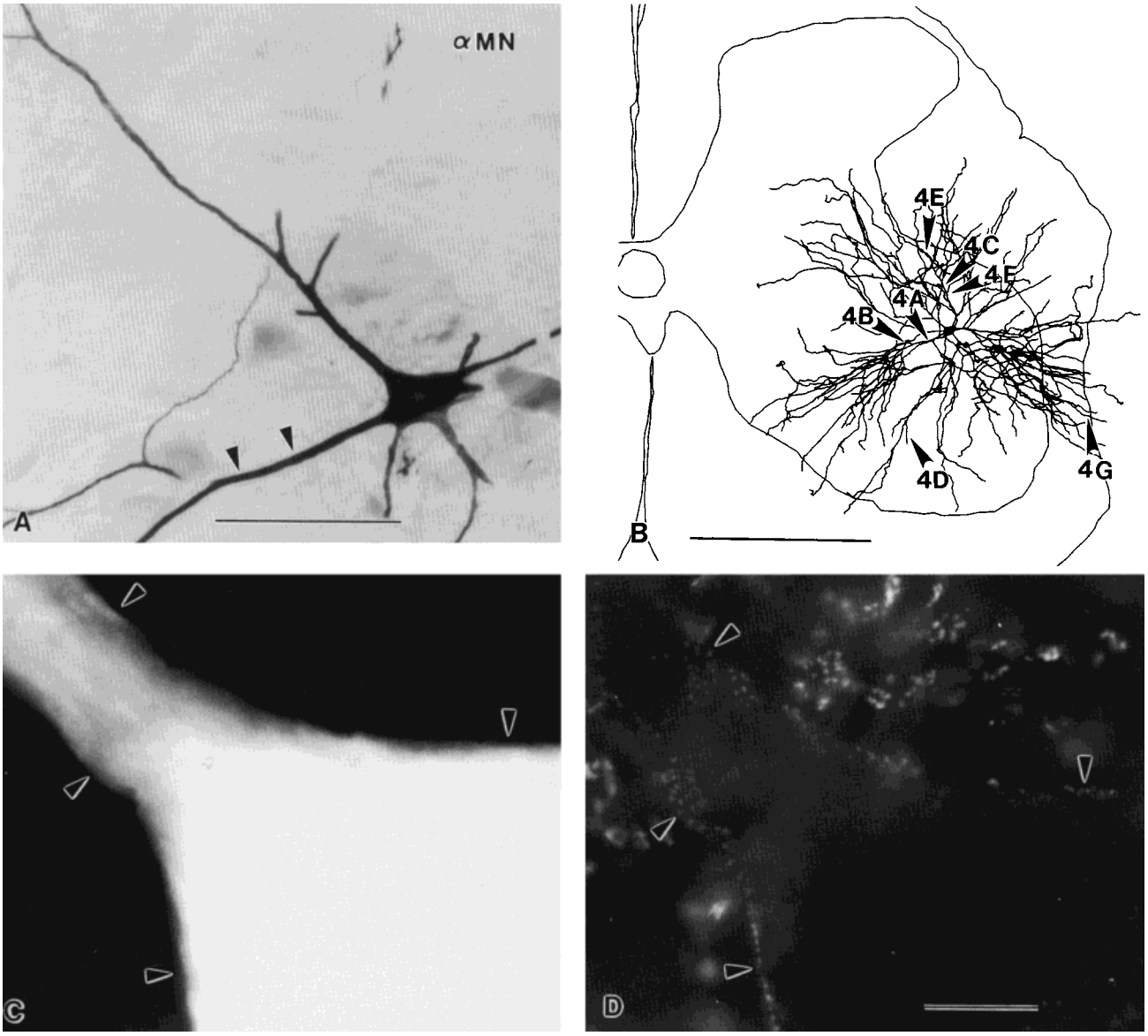

Fig. 3. Gephyrin-IR clusters on α-motoneuron (αMN) somas. **A:** Medium-magnification brightfield micrograph of the soma and proximal dendrites of the intracellularly labeled αMN shown at higher magnification and under fluorescence conditions in C and D. Two arrowheads indicate the extent of the proximal dendritic segment shown at 4A. **B:** Two-dimensional plot of the full 3D reconstruction of this αMN. For orientation purposes, the neuron reconstruction was superimposed on an outline of the L7 spinal cord section containing the cell soma. Arrowheads 4A to 4G indicate the position of dendritic segments shown in Figure 4. **C,D:** Pair of fluorescent micrographs showing the covering by gephyrin-IR clusters of the somatic and very proximal dendritic membrane. Arrowheads label the same positions in C and D. C is at the same magnification as D. Scale bars = 100 μm in A, 1 mm in B, 10 μm in D. A,C,D and B are, respectively, modified from Figs. 2, 3 of Fyffe et al. (1995) and are reproduced with permission of Plenum Press.

was generally confirmed by using a filter cube that allowed simultaneous visualization of AMCA and FITC fluorescence (Fig. 2). Nevertheless, many of the data were obtained by photographing the intracellular label and immunoreactive clusters in serial black-and-white photographs by using specific AMCA or FITC filters (e.g., see Figs. 3, 4). With this method, the masking of one fluorochrome by the other was minimized, particularly for receptor clusters at the top and bottom surfaces of strongly fluorescent dendrites.

The densest concentration of gephyrin-IR aggregates was found on αMN cell somas and more proximal dendrites (up to 150–250 μm distance; Figs. 3C,D, 4A). Indeed, these proximal regions were often effectively outlined by small immunofluorescent punctae (<0.5 μm in diameter) of rather homogeneous size and shape. Small punctae frequently organized in groups of 4–14 dots forming a circular or ellipsoidal rosette (e.g., see Fig. $4A_3$). Axon hillocks arising from somas or proximal dendrites displayed an immunoreactive covering similar to that of the adjacent somatic or dendritic membrane. Gephyrin-IR clusters were absent from the initial segment and myelinated axon.

At middle dendritic locations (from 250 to 500 μm), small immunoreactive punctae intermingled with progressively larger patches, including perforated or scalloped

profiles (Fig. 4B,C). The larger individual aggregates more commonly measured 0.7–1.5 μm along their longest diameter. The density of gephyrin-IR clusters was much lower on distal dendrites (e.g., farther than 500 μm from the cell soma) and tended to be nonuniform, with variable stretches of dendrite devoid of receptor clusters (Fig. 4D,E). At distal locations, larger gephyrin-IR complexes predominated, many of them constituting perforated patches (i.e., see Fig. $4E_2$). Interestingly, gephyrin-IR clusters were also observed on dendritic spines (which are sparsely distributed on motoneuron dendrites; see Fig. 4F) and on the varicosities and thin intervaricose segments that are characteristic of many distal motoneuron dendrites. αMN dendrites also extend into the white matter, where they taper (usually with varicose segments) and terminate; sparsely distributed gephyrin-IR clusters of various sizes and shapes were also observed at these distal locations (frequently more than 1,000 μm from the cell body; Fig. 4G).

Although gephyrin immunoreactivity on γMNs (n = 6) was less dense than that on corresponding parts of αMNs, the γMNs displayed similar somatodendritic gradients of gephyrin-IR cluster size and complexity (Fig. 5). There were several differences, however. Large gephyrin clusters were comparatively more frequent at proximal locations on γMNs than on αMNs. Also, in contrast to αMNs, a large variability in the density of gephyrin-IR clusters was found between different γMNs. The cell soma of one γMN was devoid of gephyrin-IR clusters, and there were very few clusters in its dendritic arbor. Three other γMNs displayed gephyrin-IR clusters at low densities, both on their somas and throughout their dendritic arbors. Finally, two γMNs showed higher gephyrin-IR densities on their cell somas and dendrites, approaching the density seen in αMNs. Thus, different γMNs may display very different densities of gephyrin-IR clusters in their somatodendritic arbor.

Gephyrin immunoreactivity on the soma and dendritic membranes of interneurons

Interneurons (IaINs and RCs) exhibited the highest levels of gephyrin immunolabeling observed in this study. RC (n = 4) gephyrin-IR clustering was quite different from that of any other spinal cord cell (Fig. 6). RC somas and proximal dendrites displayed predominantly gephyrin-IR clusters of great size and complex morphology. The highest concentration of gephyrin-IR clusters, many extraordinarily large, measuring from 1.5 to 3 μm along the longest axis, were found in the most proximal dendritic regions (first 100 μm adjacent to the cell soma). Immunoreactive clusters decreased in frequency quite abruptly on RC dendrites at a distance of 120–180 μm from the cell soma and were practically absent from the distal fine branches (extending up to 800 μm distal to the cell soma).

IaINs (n = 7) displayed gephyrin-IR aggregates that, on average, increased in size with distance, as occurred in MNs. Proximally and on the cell soma, gephyrin-IR aggregates were most frequently of the small punctate type. The major difference in comparison to the αMN expression pattern was a relatively higher membrane covering by gephyrin-IR aggregates in IaINs, particularly at middle and distal dendritic regions, and the occurrence of larger and more complex clusters at relatively more proximal locations (compare Fig. 4A to Fig. 7B,C). Most IaIN dendrites terminated at a distance of approximately 800–1,100 μm. Most dendritic terminations remained within the gray matter and formed beaded (varicose) dendritic segments that displayed many gephyrin-IR clusters up to and including the terminal varicosity.

Gephyrin aggregates in relation to the synaptic terminals of identified neurons

Axon collaterals of some αMNs (n = 6) and IaINs (n = 3) were extensively labeled intracellularly by neurobiotin, and their boutons could be visualized by using AMCA fluorescence. As expected, αMN terminals were unrelated to gephyrin-IR clusters, whereas almost all IaIN axon swellings were associated with one or more gephyrin-IR clusters (Fig. 7D,E). Gephyrin immunoreactivity was presumably located postsynaptically to these axon terminals. Different synaptic boutons generated by a single neuron, even boutons present along a single terminal axon branch, were associated with postsynaptic gephyrin-IR aggregates of variable sizes and configuration.

Quantitative analysis of gephyrin expression patterns

We estimated that, under these experimental conditions, our resolution limit was approximately 0.5 μm (see Materials and Methods), similar to a recent study using similar methods (Koulen et al., 1996). The smaller clusters measured 0.4–0.5 μm in diameter. However, their actual size was likely magnified by surrounding fluorescence haze. Using electron microscopy (see below), a smaller size for the smallest gephyrin-IR clusters on the somas and proximal dendrites of ventral horn neurons, 0.15–0.2 μm in diameter, can be accurately measured. Fluorescence haze and the resolution limits of light microscopy introduce an approximately 0.1–0.2 μm fuzzy surrounding to the real contours of the immunofluorescent patches. Because accurate measurement of the smallest gephyrin-IR clusters is beyond the resolution limits of light microscopy fluorescence and a similar fluorescent halo occurs around larger clusters, we grouped our data in bins of 0.5 μm to reduce any bias introduced by measurement errors. Means probably constitute overestimations of the real population (the size of small clusters is consistently overestimated), and standard deviations are probably underestimated (the smaller clusters are all "magnified" to an apparent diameter of 0.4–0.5 μm). These effects are presumably more important at proximal locations, where small clusters predominate. Nevertheless, mean and SD distributions of our data basically show the same results (see statistical analysis below and Table 1), as do the frequency distribution histograms (Fig. 8).

Gephyrin-IR aggregates in two cells from each neuronal class were measured (size of the longest axis) and classified according to distance to the cell soma (Fig. 8). In total 6,188 clusters were sampled. Neurons used for quantitative analysis were all well stained. Their morphological characteristics and plots of the distribution of their dendritic surface membrane area are represented in Figures 9 and 10. The frequency distributions of gephyrin-IR cluster sizes demonstrates the existence of a clear size gradient in that increased proportions of large gephyrin-IR clusters appear distally in the dendritic trees of αMNs, γMNs, and IaINs. Note, however, that the total number of clusters measured decreased distally (Table 1), probably because they are present at a lower density in distal regions and also because the total available surface membrane decreased with distance (Figs. 9, 10). The steepness of the cluster size gradient was greatest in IaINs, in which the

transition from predominantly small clusters to a mixture of small and large clusters was apparent within 150–200 μm from the soma. In contrast, small punctate gephyrin-IR clusters predominated up to midregions of the dendritic arbor in αMNs. It should be noted, however, that the size gradient reflects the *average* dimensions of clusters in each region. Gephyrin-IR clusters were rather homogenous proximally, but their morphological variability progressively increased with distance from the cell soma. No clear size gradient was noted in RC frequency distribution histograms.

Similar conclusions were obtained after statistical analysis (see Materials and Methods) of the trends shown by the average cluster sizes (Table 1). The effect of cell type and dendritic location on gephyrin-IR clusters sizes was analyzed by using a three-way mixed-effects ANOVA (see Materials and Methods). The overall F test indicated that there is a significant relationship between cluster size and the set of independent variables (cell type and distance; $F = 105.70$ with 21 and 6,166 degrees of freedom; $P = 0.0001$). An additional term representing the joint interaction of cell type and distance was also included in the model and was found also to be statistically significant ($F = 12.84$ with 10 and 6,166 degrees of freedom; $P = 0.0001$), suggesting that the effect of cell type on cluster size varies with distance and, likewise, that the effect of distance varies in different cell types. Thus, the somatodendritic size gradient displayed different characteristics in the different cell types. Because there is a significant joint effect of cell type and distance on cluster size, we examined the effect of cell type by each distance category separately, as well as the effect of distance in each cell type, by using two-way mixed-effects ANOVAs and Fisher's LSD multiple comparisons (see Materials and Methods).

Analysis of differences along the dendritic arbor of single cell types. The results of our ANOVA analysis indicate a significant relationship between distance and cluster size in αMNs, γMNs, IaINs ($P = 0.0001$) but not in RCs ($P = 0.1910$). In order to determine how cluster sizes differ by distance category, we conducted Fisher's LSD multiple-comparison procedures for the different distances (see Materials and Methods). For αMNs, cluster sizes differ significantly ($P = 0.0001$) for each pair of distance categories, except for the 0–100 and 100–200 μm distances from the cell soma ($P = 0.0182$). In all other cases, statistically significant differences were found, and the larger clusters were present in the category of greater distance from the cell soma. The only exception was for clusters over 1,000 μm from the cell soma that were significantly smaller than clusters in the 500–1,000 μm range but larger than all other distance categories. At these very distal ends of αMN dendritic branches, the smaller dendritic diameter and extensive tapering in the white matter might constitute additional limiting factors that affect gephyrin-IR cluster size. For γMNs, gephyrin-IR clusters in the 0–100 μm distance category were smaller and differed statistically from clusters in all other distance categories ($P = 0.0001$), but differences between pairs of more distal categories did not reach statistical significance. This result reflects the larger variability of cluster sizes and also the smaller number of clusters found in these cells for each distance category. Moreover, there were very large differences between the two γMNs in the number of gephyrin-IR clusters displayed. In contrast, both IaINs displayed rather similar dendritic arbors and patterns of gephyrin-IR clustering. Our statistical analysis showed that IaIN gephyrin-IR cluster sizes differ significantly for each pair of distance categories ($P = 0.0001$), except for the 500–1,000 μm with the over 1,000 μm category ($P = 0.0892$). This result parallels the "steeper" size gradient on IaINs in comparison to that on αMNs. It also represents the fact that IaIN dendrites are usually shorter than αMN dendrites and that they frequently end with a few varicosities inside the ventral horn gray matter and do not taper extensively in the white matter. Hence, IaIN gephyrin-IR cluster size average increases seem to reach a plateau after 500 μm.

Analysis of differences in cluster size for each dendritic distance due to cell type. The results of our ANOVA analysis (using cell type and individual cell as factors) indicate that cluster size varies significantly by cell type in the 100–200 μm distances ($P = 0.0068$) and also marginally in the 0–100 μm distances ($P = 0.0107$). Fisher's LSD multiple-comparison procedures between the average cluster sizes of the different cells in the different distance categories revealed that gephyrin-IR clusters on RC dendrites were statistically different at 0–100 and 100–200 μm from the cell soma in comparison to those on αMNs ($P = 0.0042$ and $P = 0.0047$, respectively) and IaINs ($P = 0.0038$ and $P = 0.0052$, respectively). Gephyrin-IR clusters were also significantly different for γMNs in the 0–100 μm distance category ($P = 0.0089$), but the difference did not reach statistical significance in the 100–200 μm distance category ($P = 0.6721$), most likely because of the large internal variability of the γMN sample at this distance. Finally, no statistically significant differences were found between different cells at distances farther than 200 μm from the cell soma. This result is somewhat surprising, because the average size of RC clusters is considerably larger in the 200–500 μm distance category than it is in all other cells. The small numbers of RC clusters sampled at this distance and the internal variability within each cell type are probably responsible for the result we obtained with our statistical model. In conclusion, our analysis indicates 1) that distance and cell type are jointly related to cluster size, 2) that the relationship between distance and cluster size exhibits different characteristics in different neurons, 3) that RCs do not display a relationship between distance and cluster size, and 4) that proximal gephyrin-IR clusters are significantly different in RCs in comparison to those in other cells.

Fig. 4. Gephyrin-IR clusters on selected α-motoneuron (αMN) dendritic segments indicated in Figure 3. A–G contain dendritic segments photographed first to reveal AMCA fluorescence and then gephyrin immunofluorescence. Arrowheads indicate the position of selected gephyrin clusters in both micrographs. Asterisks indicate the approximate position where the indicated distance to the cell soma was measured. Arrows indicate the directions in which the cell somata are located. **A:** Proximal dendrite densely covered by gephyrin-IR clusters; A_1 shows the intracellularly labeled dendritic segment; A_2 shows a middle focal plane through the dendrite, rendering a side view of gephyrin-IR clusters on the membrane; A_3 shows a superficial focal plane rendering an en face view of the organization of proximal dendritic clusters. Proximal gephyrin-IR clusters are frequently organized in rosettes (arrows). **B,C:** Gephyrin-IR clusters in middle regions of the dendritic arborization. **D,E:** Gephyrin-IR clusters in distal regions of the dendritic arborization become larger and more sparsely distributed. Note in E a typical large perforated patch. **F:** Gephyrin-IR clusters in the neck and head of a dendritic spine. **G:** Large gephyrin-IR clusters in a very distal white matter dendrite. All micrographs are at the same magnification. Scale bar = 10 μm.

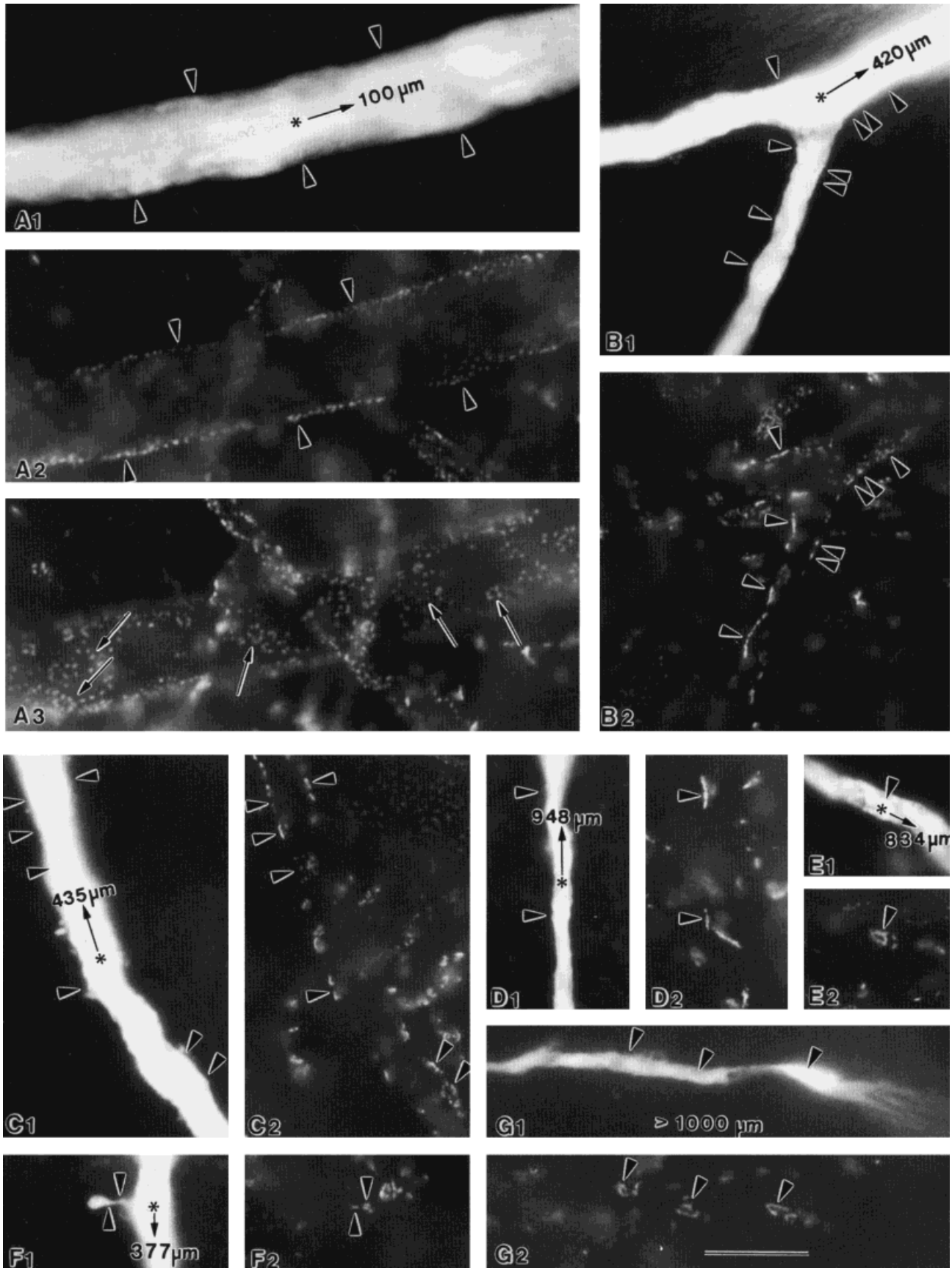
100 µm
A1
A2
A3
420µm
B1
B2
435µm
C1
C2
948 µm
D1
D2
834µm
E1
E2
377µm
F1
F2
> 1000 µm
G1
G2

Figure 4

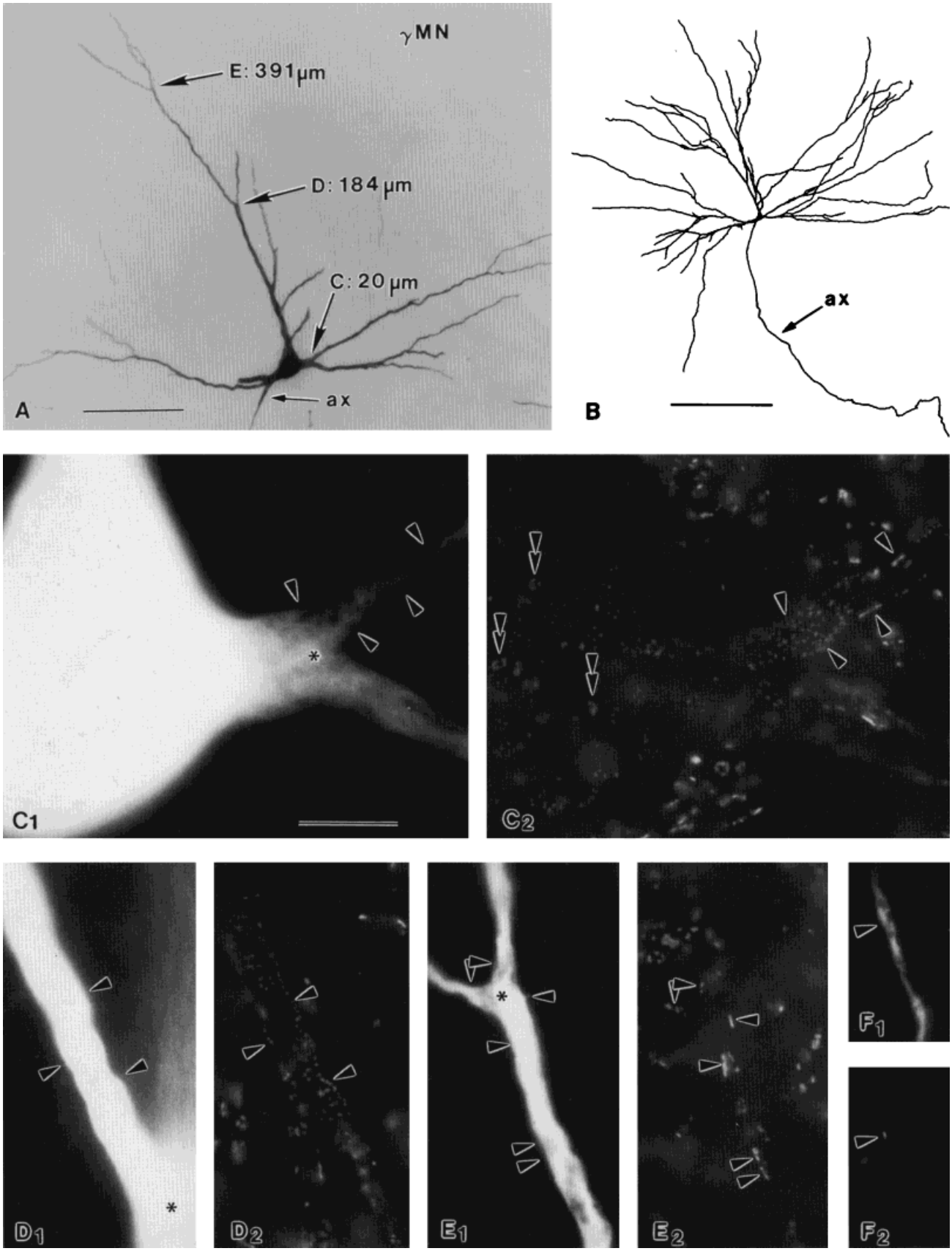

Fig. 5. Gephyrin-IR clusters over the somatodendritic surface of a γ-motoneuron (γMN). **A:** Intracellularly filled γMN. The locations and distances to the cell soma of dendritic segments shown in C–E are indicated. **B:** Reconstruction of the dendritic arborization and initial axon trajectory. The axon hillock and axonal trajectory are indicated as ax in A and B, respectively. **C–F:** Pairs of high-magnification micrographs showing first AMCA intracellular fluorescence and then gephyrin-IR clusters. Asterisks in C–E show the locations indicated and measured in A. F shows a dendritic segment located in the white matter at a very distal location in the dendritic tree (more than 1,000 μm). Matching arrowheads indicate the position of selected gephyrin-IR clusters for each pair of photographs. Double arrowheads in C_2 indicate relatively large clusters found on the surface of γMN cell bodies. C–F are at the same magnification. Scale bars = 100 μm in A, 500 μm in B, 10 μm in C_1.

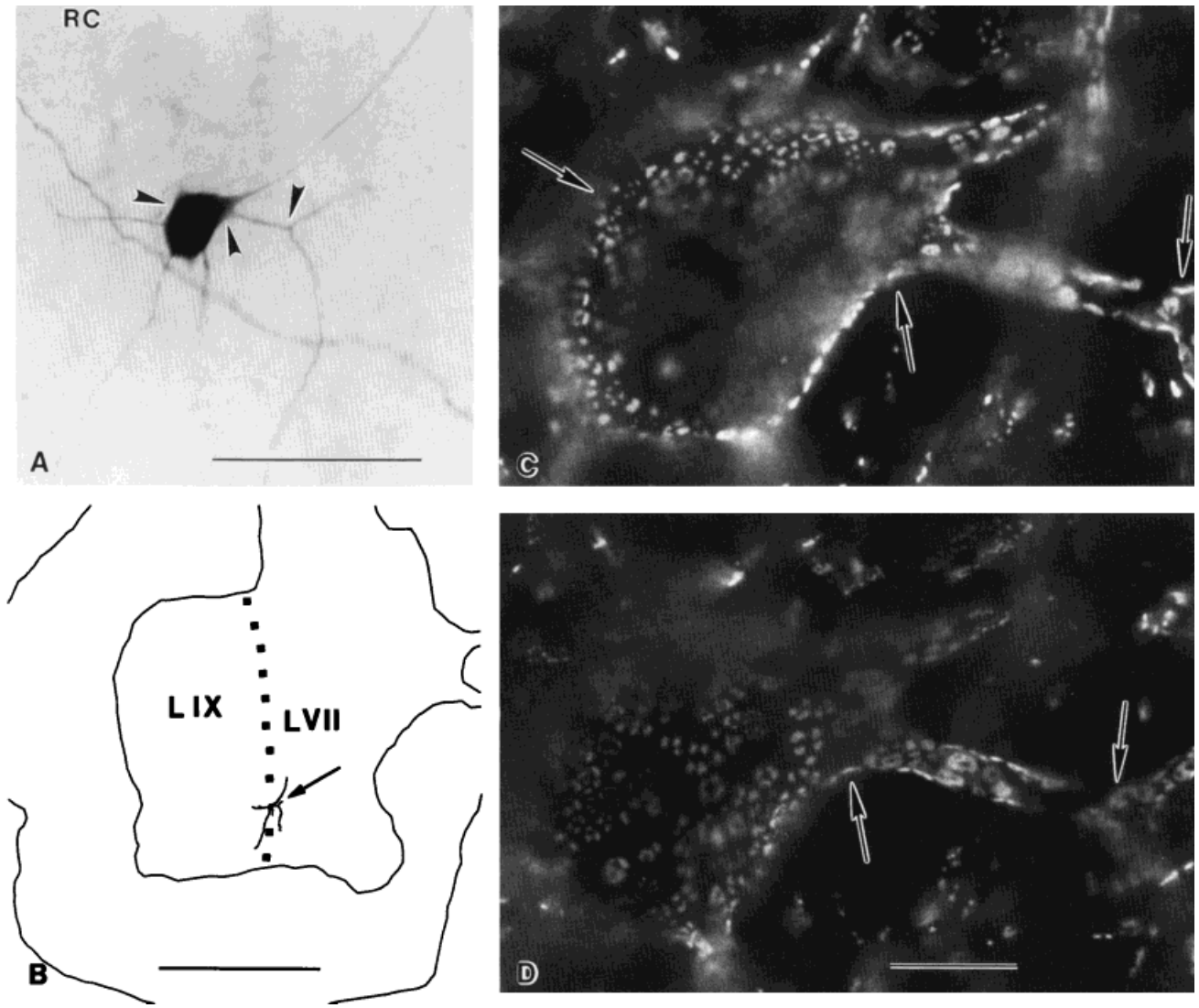

Fig. 6. Gephyrin-IR clusters over the cell soma and proximal dendrites of a Renshaw cell (RC). **A:** Brightfield micrograph of an intracellularly filled RC. Arrowheads indicate approximately the same location as arrows in C and D. **B:** Reconstruction of the dendritic filling of RC in A. The cell reconstruction was superimposed within an outline of the spinal cord, pointing to the approximate boundary of laminae IX and VII. **C,D:** High-magnification micrographs of gephyrin-IR clusters obtained at two different focal planes of the RC soma and proximal dendrites. C is at the same magnification as D. Scale bars = 100 μm in A, 500 μm in B, 10 μm in D.

Ultrastructure of gephyrin-IR patches

By using electron microscopy, we analyzed over 1,000 cross sections of individual gephyrin-IR patches sampled from the spinal cord ventral horn (Fig. 11) and a smaller sample (n = 23) of serially sectioned and reconstructed synaptic boutons that face postsynaptic gephyrin-IR patches on putative αMN and RC somas (Fig. 12). αMN somas were identified as cell bodies located in lamina IX displaying diameters larger than 45 μm; RC somas were identified based on their characteristic and unique complement of very large gephyrin-IR clusters and their location in ventral lamina VII. The ultrastructural analysis clearly demonstrated that 1) all gephyrin-IR clusters were restricted to postsynaptic sites, independently of their size or morphological configuration; 2) simple or complex configurations of gephyrin-IR clusters at these synapses correspond with similar morphologies in their respective presynaptic active zones (defined as the presynaptic membrane area associated with an accumulation of synaptic vesicles and juxtaposed to a synaptic cleft; Fig. 12); and 3) the areas of somatic postsynaptic gephyrin-IR patches in RCs are, on average, approximately ten times larger than somatic αMN gephyrin-IR patches. We also noted that the ultrastructural dimensions of small gephyrin-IR clusters frequently fell below the resolution limits of our fluorescence preparations (estimated at approximately 0.5 μm).

The results indicate that the large and complex gephyrin-IR patches detected with immunofluorescence most likely represent postsynaptic regions apposed to presynaptic active zones that display similar configurations and occupy large regions of the apposition area between the presynaptic terminal and the postsynaptic membrane. Eleven boutons with complex postsynaptic gephyrin-IR patches were fully reconstructed in serial sections from the

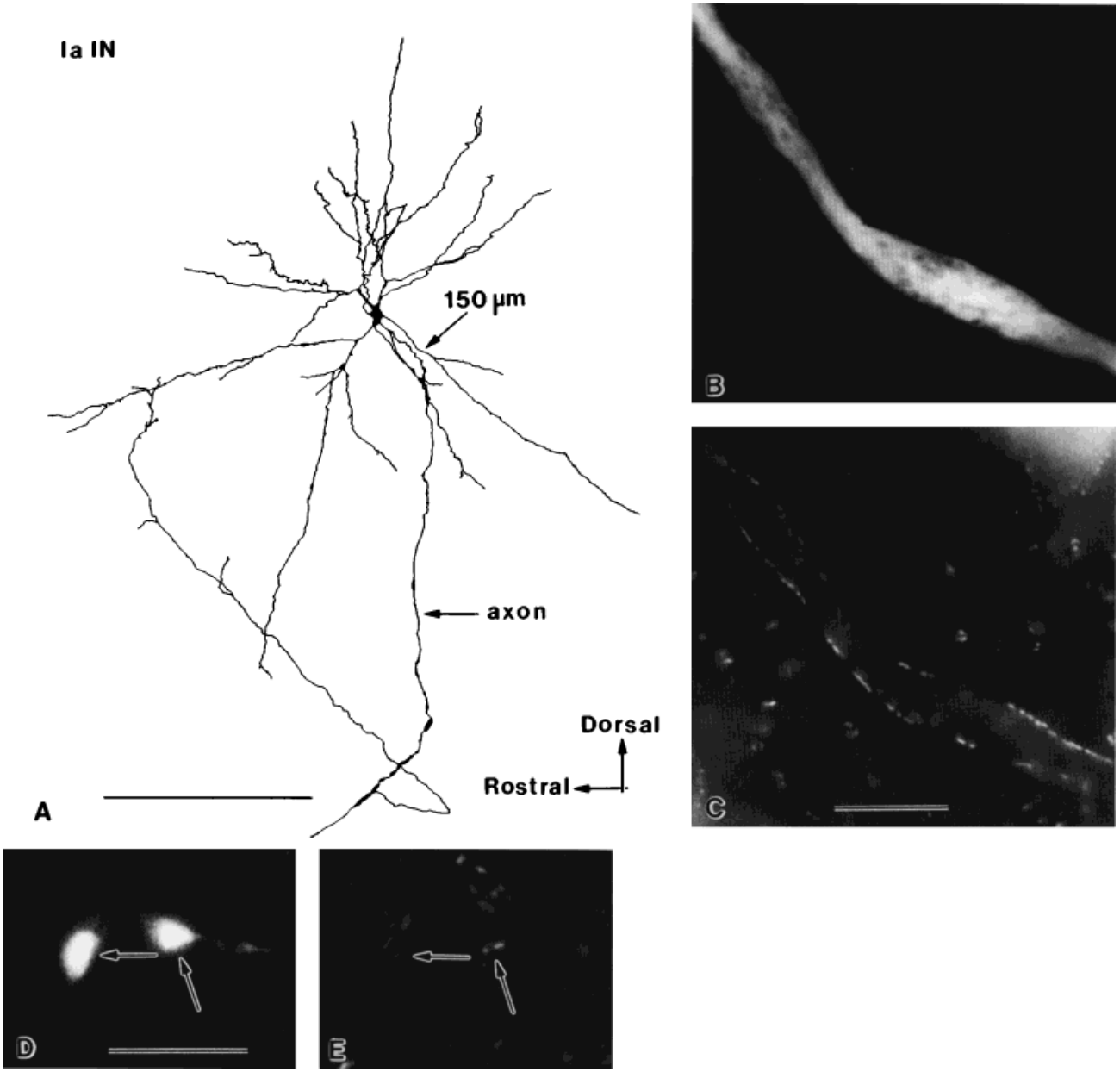

Fig. 7. Gephyrin-IR clusters associated with Ia inhibitory interneurons (IaINs). **A:** Parasagittal 2D view of the cell body and dendritic arborization of a IaIN. Orientation is indicated at lower right. Arrows indicate the location and distance to the soma of the dendritic segment displayed in B and C. The initial trajectories of the IaIN axon and one collateral are also shown. **B,C:** Pair of high-magnification micrographs of the proximal dendritic segment indicated in A, showing AMCA intracellular fluorescence (B) and a high density of relatively large gephyrin-IR clusters (C). **D,E:** Gephyrin-IR clusters (E) in relation to synaptic boutons of IaIN axon collaterals (D). E shows en face (left arrow) and side (right arrow) views of gephyrin-IR clusters associated with two consecutive synaptic varicosities (arrows in D). In en face views, gephyrin-IR clusters and labeled varicosities lie at slightly different focal planes, but the side-on views of gephyrin-IR clusters are clearly located outside and opposing the adjacent labeled varicosities. B and C are at the same magnification, and E and D are at the same magnification. Scale bars = 500 µm in A, 10 µm in C,D.

surface of a putative RC soma. Each bouton displayed one independent gephyrin-IR cluster. The reconstructed gephyrin-IR postsynaptic patches were all relatively large. The largest cross section through each gephyrin-IR patch measured in the electron microscope ranged from 0.69 to 1.78 (1.19 ± 0.38, mean ± S.D.). Because of their complexity, "the longest cross section" frequently does not represent the "true" longest axis of the gephyrin-IR cluster as visualized with fluorescence. Longest lengths of the 2D projected reconstructed areas (Fig. 11) ranged from 0.78 to 2.03 µm (1.38 ± 0.46, mean ± S.D.). Eight gephyrin-IR clusters (72.72%) measured more than 1 µm. The 2D projection areas of postsynaptic gephyrin immunoreactivity in RCs measured from 0.21 to 2.14 μm^2 (1.00 ± 0.63, mean ± S.D.).

Other glycinergic synapses contained multiple small, simple active zones, again probably corresponding to the punctae observed with immunofluorescence. Frequently,

TABLE 1. Means and Standard Deviations of Gephyrin-IR Cluster Sizes Measured at Different Distances from the Cell Soma***

	Distance				
Cell type	0–100 μm	100–200 μm	200–500 μm	500–1000 μm	>1000 μm
αMNs (n = 2)*	0.53 ± 0.17 (425)**	0.55 ± 0.20 (862)	0.73 ± 0.44 (1,059)	1.09 ± 0.63 (609)	0.83 ± 0.51 (94)
γMNs (n = 2)	0.57 ± 0.29 (403)	0.62 ± 0.29 (128)	0.72 ± 0.39 (283)	0.81 ± 0.45 (235)	1.06 ± 0.39 (16)
IaINs (n = 2)	0.55 ± 0.18 (508)	0.68 ± 0.30 (420)	0.87 ± 0.45 (541)	1.08 ± 0.59 (370)	1.22 ± 0.46 (25)
RCs (n = 2)	1.40 ± 0.76 (148)	1.48 ± 0.69 (39)	1.64 ± 0.70 (23)	n.d.	n.d.

*Number of cells analyzed.
**Number of independent gephyrin-IR clusters measured. The numbers are very different in different regions, usually reflecting the dendritic surface membrane area and the different density of gephyrin-IR clusters in each region.
***Note that clusters smaller than 0.4–0.5 μm are beyond the resolution limit of the techniques used and therefore this data reflect only approximations to the real values as explained in the text.

small immunofluorescence dots formed rosettes of small punctae that ultrastructurally were identified as corresponding to single presynaptic boutons establishing multiple small, separate, synaptic active zones within a much larger apposition region. For example, 12 synaptic boutons on αMN somas were fully reconstructed in serial sections. These 12 boutons displayed a total of 39 independent gephyrin-IR patches, most of which were approximately circular in shape and considerably smaller than those reconstructed from RC somas. The largest cross sections, measured from individual electron micrographs, ranged from 0.13 to 1.45 μm (0.41 ± 0.20, mean ± S.D.). In reconstructed 2D projections of MN gephyrin-IR patches, the longest axis measured from 0.13 to 1.55 μm (0.43 ± 0.22, mean ± S.D.). The majority (84.6%) had diameters smaller than 0.55 μm, and more than half of these (56.41%) were smaller than 0.40 μm. Postsynaptic gephyrin-IR areas measured from 0.01 to 0.71 μm^2 (0.11 ± 0.1, mean ± S.D.).

DISCUSSION

The single-cell analysis pursued in this study made possible three interesting observations. First, postsynaptic glycine receptor clusters occur in a wide range of shapes and sizes in individual neurons, and the organization of this morphological complexity varies along the dendritic trees of different neurons. Second, for most neurons (αMNs, γMNs, and IaINs), glycine receptor clusters are, on average, larger and of more complex configuration at distal dendritic sites. Third, RCs display a specialized pattern of postsynaptic receptor organization at glycinergic synapses. However, we must first discuss the validity of the use of gephyrin immunoreactivity to study morphological aspects of glycine receptor clustering.

Gephyrin immunoreactivity and glycine receptor localization in ventral horn neurons

Colocalization of gephyrin and glycine receptor α-subunits was previously reported for spinal neurons in situ (Triller et al., 1985, 1987; Kirsch and Betz, 1993) and in culture (Kirsch et al., 1993). Moreover, the relationship between gephyrin and glycine receptor clustering has been well characterized in vitro, leading to the suggestion that gephyrin is involved in anchoring postsynaptic glycine receptor complexes by bridging β-subunits of the receptor to cytoskeletal structures (Kirsch et al., 1993; Kirsch and Betz, 1995; Meyer et al., 1995). However, in some instances, gephyrin has also been shown to have a more widespread distribution than known ligand-binding subunits of the glycine receptor, suggesting that it could also be related to other, as yet uncharacterized, receptor molecules (Kirsch and Betz, 1993; see also Meyer et al., 1995). Therefore, in the present study, we had to reassess the validity of analyzing gephyrin immunoreactivity for studying the structural features of receptor clustering at glycinergic synapses in ventral horn neurons. By using sequential double immunofluorescence for α_1-subunits and gephyrin, we concluded that the location and extension of gephyrin immunofluorescence broadly coincided with the location and extension of α_1-subunit patches. Carefully designed controls were used to avoid artifactual colocalization. Our results corroborated earlier conclusions (Triller et al. 1987) that there is good colocalization between gephyrin and α_1-subunits on ventral horn neurons and the results of Todd et al. (1995), which demonstrated an excellent match between presynaptic glycine and postsynaptic gephyrin immunoreactivity at ventral horn synapses.

In our preparations, α_1-subunit immunoreactivity was frequently found to be more abundant at the periphery of the gephyrin-IR cluster. This result differs from a related observation made by Triller et al. (1990) on the Mauthner cell. In the latter study, immunoreactivity against mAb 4a (which cross-reacts with various α- and β-subunits; Schröeder et al., 1991; Kirsch and Betz, 1993) was found to be more prominent in the center of the patch. However, this antibody (mAb 4a) gave inconsistent results in our cat spinal cord preparations (unpublished observations). Our results with mAb 2b could indicate that α_1-subunits of the glycine receptor are more abundant in the periphery of gephyrin-IR patches, but alternatively this could also be due to failure to obtain uniform penetration of the antibodies throughout the synaptic clefts; mAb 2b is directed against an extracellularly located epitope of the α_1-subunit (Schröeder et al., 1991; Triller et al., 1985), so glycine receptors at the center of the synaptic active zones might have their epitopes partially masked by the complex macromolecular matrix filling the synaptic cleft.

Variability of gephyrin/glycine receptor clustering

A somatodendritic gradient was found for αMNs, γMNs, and IaINs, in that small clusters concentrate proximally, whereas clusters are larger and more complex distally. Based on our observations of the overall patterns of gephyrin immunoreactivity observed in the neuropil, we conclude that most ventral horn neurons follow similar rules of clustering along their dendritic arbors. A size and complexity gradient for glycine receptor clusters similar to that reported in this paper has been observed on the Mauthner cell of teleost fish (Triller et al., 1990). These gigantic neurons display two large and specialized dendrites, one oriented ventromedially and the other dorsolaterally, and a number of smaller cap dendrites dorsal to the cell soma. The ventromedial and dorsolateral dendrites

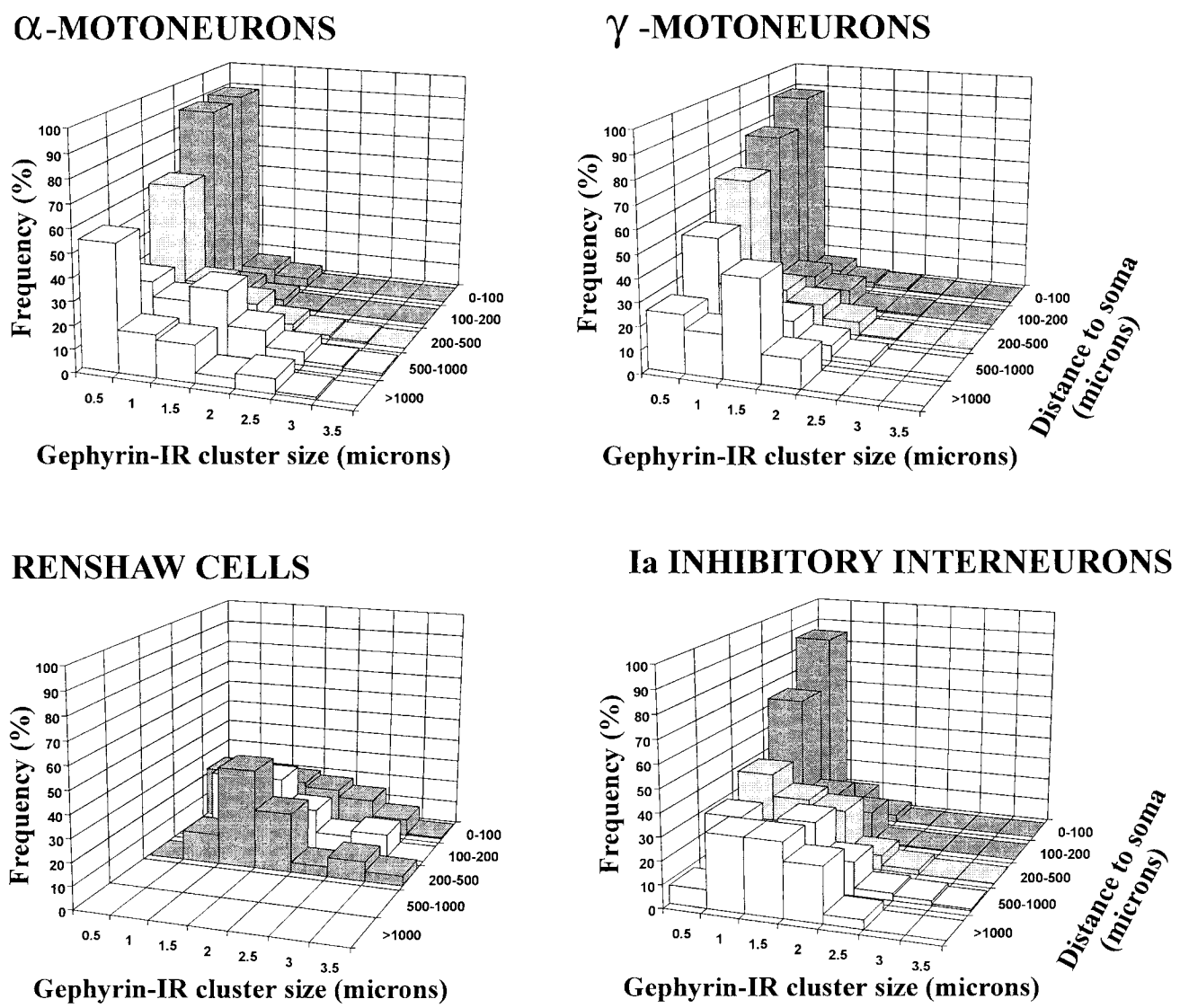

Fig. 8. Quantitation of gephyrin-IR cluster sizes in the dendritic arbors of motoneurons and interneurons; 3D bar histograms represent the frequency (y axis) of different sizes of gephyrin-IR clusters (x axis) found in dendritic segments located at different distances from the cell soma (z axis). Gephyrin cluster sizes were grouped in 0.5 μm bins according to the length of their longest axis. In total, 3,049 clusters were measured on α-motoneuron dendrites, 1,065 on γ-motoneuron dendrites, 1,864 clusters on Ia inhibitory interneuron dendrites, and 210 on Renshaw cell dendrites. A somatodendritic gradient of gephyrin-IR cluster sizes along the dendrites of both types of motoneurons and Ia inhibitory interneurons is apparent. IaINs display a somatodendritic gradient "steeper" than that of motoneurons. Renshaw cells show no evidence of a somatodendritic gradient.

displayed size gradients similar to those reported in this paper, whereas the clusters in cap dendrites were uniformly small. In the present study, we found that a size gradient in glycine receptor clustering is probably also a prominent feature of the dendritic arbors of many types of mammalian neurons, although there are notable exceptions (i.e., RCs). Our observations, thus, extend the generality of the data obtained in the Mauthner cell (Triller et al., 1990). There is also ultrastructural evidence that active zone sizes for excitatory Ia afferent terminals on motoneurons may be larger on distal than on proximal dendrites (Pierce and Mendell, 1993). Interestingly, Calverley and Jones (1990) and Lisman and Harris (1993) have reviewed evidence indicating that the morphological complexity of presynaptic active zones and postsynaptic densities correlates with measures of synaptic efficacy. Systematic increases in receptor cluster size and structure, as seen in this study, possibly result in increased receptor channel numbers and/or density at distal dendritic synapses. If released neurotransmitter caused the opening of more channels at distal synapses, the observed size gradient might represent a mechanism to compensate, at least partially, for the electrotonic attenuation that affects synaptic potentials generated at distal synaptic locations (see, e.g., Rall et al., 1992; Spruston et al., 1994).

The exact functional significance of this structural variability is, however, difficult to interpret based on present knowledge of central synaptic mechanisms. One important factor yet unresolved is the amount of postsynaptic receptor activation and/or saturation obtained after quantal or multiquantal release at central synapses (reviewed in Redman, 1990; Korn and Faber, 1991; Trussell et al., 1993;

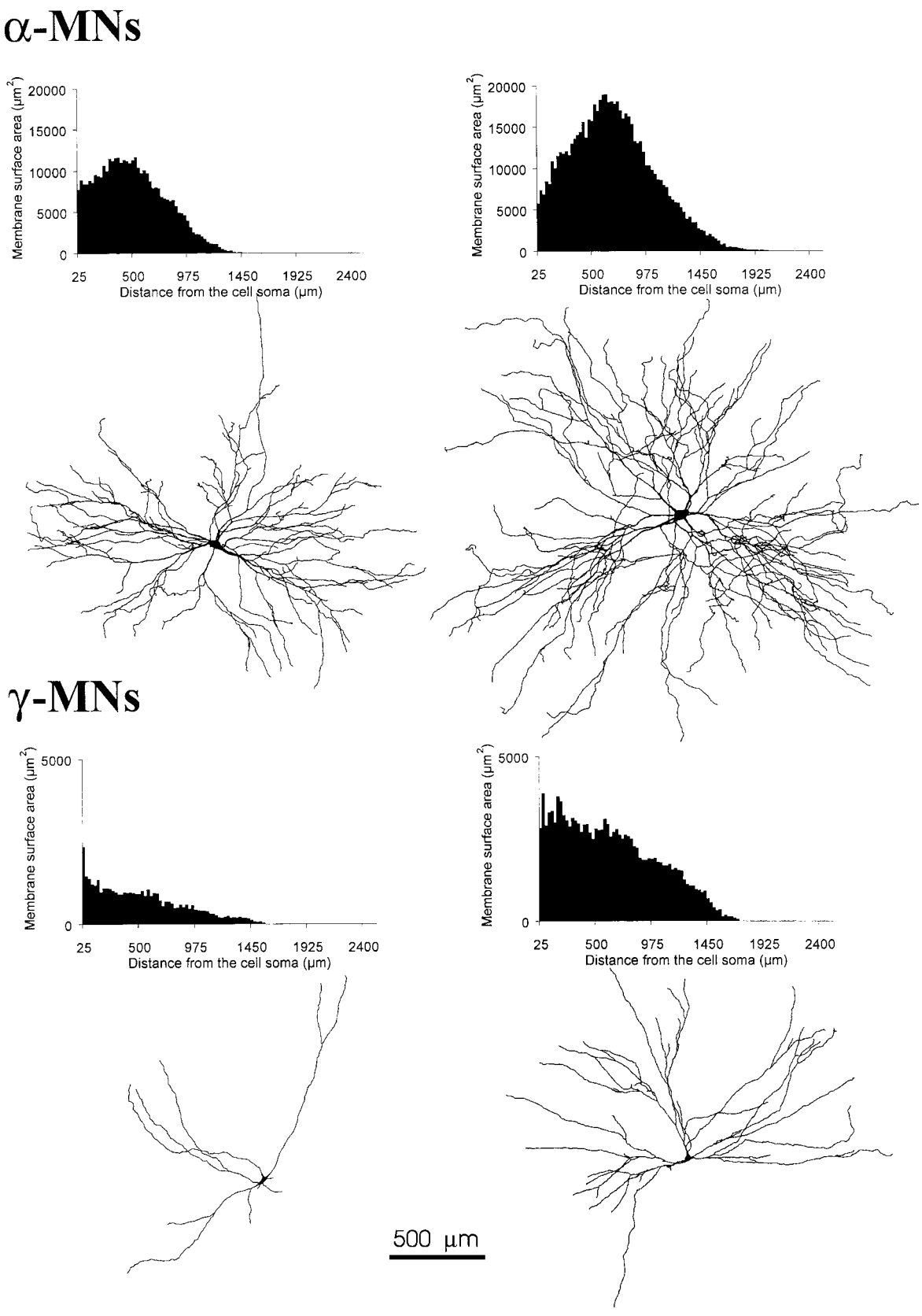

Fig. 9. Reconstructions of the dendritic arborizations of α- and γ-motoneurons included in the sample for quantitative analysis of gephyrin-IR clusters. Different neurons displayed different amounts of available surface membrane, as shown in the associated histograms. Histograms show plots of the distribution of aggregate membrane area per 25 μm of dendritic length as a function of path distance from the soma. Both α-motoneurons displayed similar covering by gephyrin-IR clusters and similar somatodendritic gradients. The γ-motoneuron represented at bottom right had a much more extensive dendritic arborization and displayed a much higher density of gephyrin immunoreactivity than the simpler one represented at bottom left. Both γ-motoneurons, however, showed similar somatodendritic gradients. All neurons are shown at the same magnification. Scale bar = 500 μm.

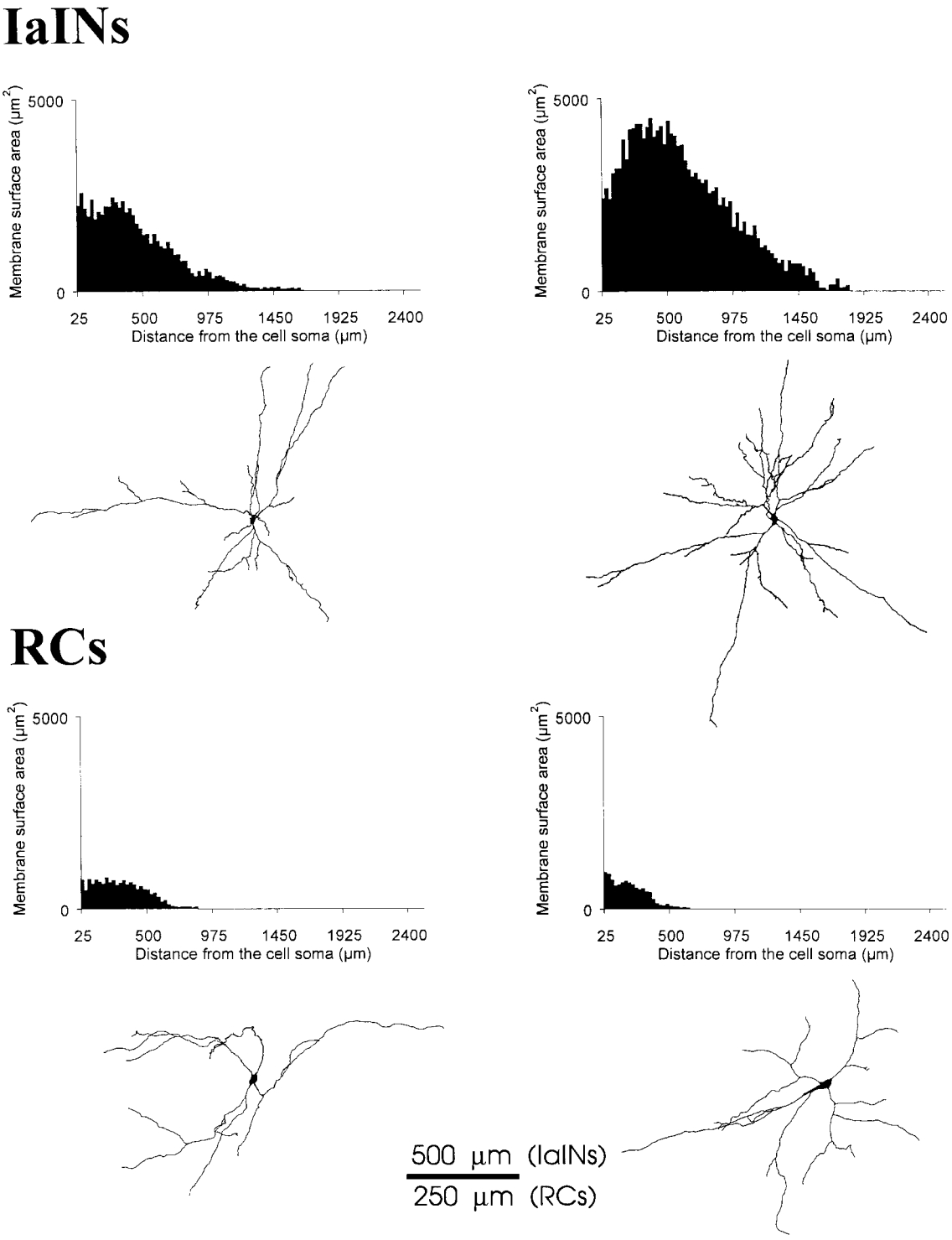

Fig. 10. Reconstructions of the dendritic arborizations of Ia inhibitory interneurons (IaINs) and Renshaw cells (RCs) used for quantitation. Distribution of membrane area is shown in the histograms as in Figure 9. RCs are much smaller and have more compact dendritic trees than all other neurons studied (note that they are represented at a magnification two times that of the other neurons). Nevertheless they displayed the largest gephyrin-IR clusters, all of which were located at very proximal locations. IaINs are similar in size to γ-motoneurons, but they express a much larger complement of gephyrin-IR clusters. They are represented at the same size as the motoneurons in Figure 9. Scale bar = 500 μm for IaINs, 250 μm for RCs.

Walmsley, 1993; Bekkers, 1994; Tong and Jahr, 1994; Holmes, 1995). The fact that gephyrin-IR patches vary so greatly in size creates the possibility that different postsynaptic receptor patches experience different degrees of saturation after neurotransmitter release. In addition to possible postsynaptic effects, there may also be consider-

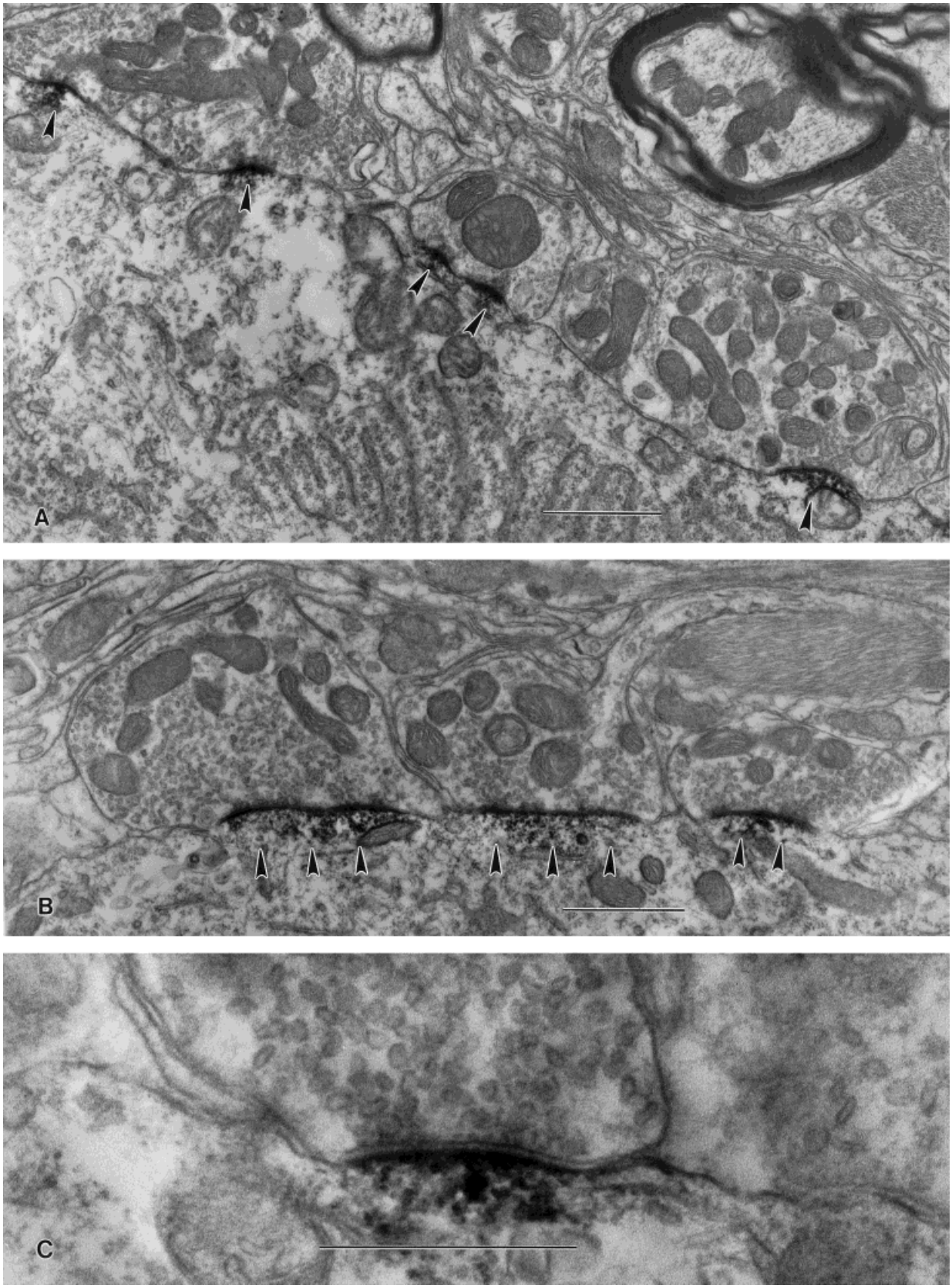

Fig. 11. Ultrastructure of gephyrin-IR clusters. **A:** Electron micrograph of a motoneuron somatic membrane region contacted by three boutons establishing various small independent synaptic contacts displaying postsynaptic gephyrin immunoreactivity (arrowheads). **B:** Electron micrograph of a somatic membrane segment from a ventral lamina VII neuron that displayed gephyrin-IR patches characteristic of Renshaw cells. This region is contacted by three boutons establishing synaptic contacts through large active zones with extensive postsynaptic gephyrin immunoreactivity (arrowheads). **C:** High-magnification electron micrograph showing the close correlation between the extension of the presynaptic releasing active zone (region displaying a presynaptic vesicle accumulation), synaptic cleft (the enlarged and more electron-dense intercellular space between presynaptic active zone and postsynaptic receptor cluster), and postsynaptic gephyrin immunoreactivity. Scale bars = 1 μm in A,B, 0.5 μm in C.

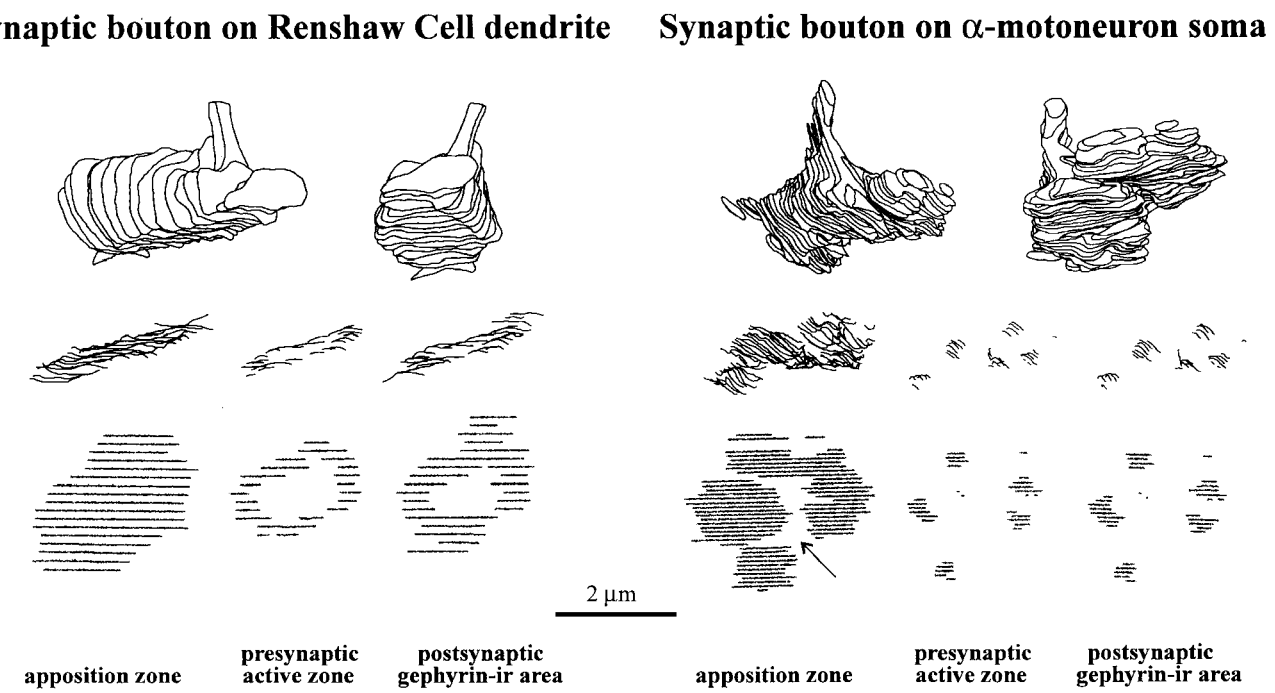

Fig. 12. Serial section reconstructions of two terminals (shown in two different rotations), sampled from a motoneuron somatic membrane (right) and a dendrite of a lamina VII neuron with Renshaw cell-like gephyrin-IR clusters (left). Second and third rows show the reconstructed zones of apposition between the terminal and postsynaptic element, the extension of the presynaptic active zone, and the extension of postsynaptic gephyrin immunoreactivity. The same areas are shown in the second row in the same orientation as the left image of the reconstructed terminals. The third row is rotated to reveal en face views of all three areas. The terminal over the motoneuron cell soma displayed a number of small independent active zones with corresponding small postsynaptic gephyrin-IR patches. Arrow, indicates a region where pre- and postsynaptic membranes separate because of an invagination of the presynaptic membrane. The terminal over the proximal dendrite of a putative Renshaw cell displays a larger and more complex active zone, including a perforation at its center, and this appears reflected in the distribution of postsynaptic gephyrin immunoreactivity.

able differences in the transmitter release properties between synaptic specializations associated with large or small gephyrin-IR clusters. Electron microscopy of gephyrin-IR patches demonstrated their excellent correspondence with the size and morphology of the presynaptic active zone. Therefore, a larger and more complex gephyrin-IR cluster indicates the presence of a larger and more complex presynaptic active zone containing more docked and, perhaps, more activated "ready-to-release" vesicles. In this context, larger gephyrin-IR patches could be associated with synapses that have an increased probability of release and perhaps also an increased frequency of multiquantal events. As a corollary of this suggestion, the observed increase in structural variability in middle and distal regions of the dendritic arbors implies that there could be considerable variability of synaptic effects among different release sites located at middle to distal electrotonic locations. Finally, smaller gephyrin-IR clusters are usually grouped in rosettes. With electron microscopy, we showed that rosettes reflect the organization of multiple independent active zones from one presynaptic bouton. Therefore, our results also suggest a predominance of glycinergic synapses with numerous multiple active zones at proximal locations.

It could be argued that different gephyrin-IR aggregates (e.g., small vs. large) are associated with different types of inhibitory synapses originating in different interneurons. However, synaptic boutons from individual axons of glycinergic interneurons (IaINs) were associated with postsynaptic gephyrin-IR aggregates of variable sizes and configurations, even when the boutons lie adjacent to each other along a single terminal axon branch. Interterminal ultrastructural variability is also present in excitatory axons (Nicoll and Walmsley, 1991; Pierce and Mendell, 1993). This finding suggests that, whereas synaptic boutons may experience similar patterns of neural activity (assuming that action potentials invariably invade all adjacent boutons), the structural features of their synapses are regulated differentially, perhaps more strongly influenced by the characteristics of the postsynaptic target.

Cell-type specific patterns of gephyrin/glycine receptor clustering

Different types of neurons clearly express different densities and organization of gephyrin-IR clusters throughout their dendritic arbors. The highest densities were seen over the surface of identified inhibitory interneurons, suggesting that these cells (which are themselves glycinergic) are subject to more substantial glycinergic input than motoneurons. Some glycinergic input to these cells is expected, because both IaINs and RCs are known to receive inhibitory input from RCs (Ryall, 1970; Hultborn et al., 1971). In addition, both IaINs (reviewed in Baldissera et al., 1981; Jankowska, 1992) and RCs (see below) receive a variety of inhibitory influences from other, as yet uncharacterized, interneurons powerfully controlled by segmental and descending inputs.

Larger clusters were observed relatively more proximal to the somas of IaINs, compared to those in αMNs, perhaps

also as a mechanism to provide a more powerful glycinergic input to these interneurons than to αMNs. However, RCs expressed the most specialized postsynaptic receptor organization found in this study. These cells expressed a large complement of very large clusters concentrated proximally. Gephyrin clusters on RCs somas and proximal dendrites are at least one order of magnitude larger in area than proximal clusters displayed by other neurons. In contrast, RCs are smaller than αMNs, γMNs, and IaINs in terms of membrane surface area. The large size of the postsynaptic receptor clusters, their very proximal locations, and the relatively smaller size of RC dendrites all suggest a much larger effect of individual glycinergic synapses in RCs than in other neurons, provided that Cl^- currents through individual glycine receptors are of relatively similar characteristics in all neurons. The origin of this impressive glycinergic input onto RCs remains unknown (although some may arise from other RCs; Ryall, 1970), but it presumably exerts an important control on RC firing. Given the very strong synaptic linkage between single motoneuron action potentials and RCs (Ross et al., 1976; Van Keulen, 1981), powerful inhibitory systems are probably necessary to maintain the RCs' role as "variable gain modulators" (Hultborn et al., 1979) of motoneuron output. Otherwise, motoneuron firing during the execution of motor behavior would consistently evoke powerful firing in RCs through motoneuron recurrent collaterals. However, segmental afferent activity and a large number of descending systems, acting upon a "local RC-inhibiting system," can indeed effectively modify the input-output relationship between RCs and MN recurrent axons (for references, see Baldissera et al., 1981; Mazzochio et al., 1994). Synaptic contact from MN recurrent collaterals is a unique and prominent feature of RCs compared to other ventral horn interneurons, perhaps suggesting that the specialized clustering of glycine receptors in RCs might have developed to counteract this particular input.

The extent of distribution of gephyrin-IR clusters in αMN dendrites was also somewhat surprising. IaIN and RC inputs over αMNs have been mapped with reasonable accuracy to the more proximal parts of the dendritic tree. Most RC synapses (94%) appear to be located less than 500 μm from the cell soma (Fyffe, 1991a), and most IaIN synapses have also been proposed to occur predominantly at juxtasomatic locations (Burke et al., 1971; Fyffe, unpublished results). These locations correspond well with those displaying the highest densities of gephyrin-IR clusters on αMNs; however, many other clusters are also seen more distally and might be presumably associated with additional glycinergic inputs from undefined sources. Glycine-containing interneurons are in fact very abundant in the ventral horn (Todd and Sullivan, 1990), and evidence for several alternative spinal cord glycinergic interneurons actively involved in MN control by using monosynaptic connections has been recently characterized electrophysiologically (Jankowska, 1992). A widespread localization of glycinergic receptors suggests that they are also involved in the fine tuning of synaptic information arriving in distal branches as well as in controlling neuronal firing as a whole through the extensive proximal complement of postsynaptic clusters.

γMNs dendrites display comparatively less covering by gephyrin-IR clusters. This observation presumably reflects the comparably weaker glycinergic input received by γMNs (reviewed in Baldissera et al., 1981; see also Ellaway and Murphy, 1981; Appelberg et al., 1983a–d). Correspondingly, immunocytochemically detected glycinergic terminals have been found more frequently over the cell somas of cat lumbar αMNs vs. γMNs (Destombes et al., 1992). It is interesting that our finding of a higher density of gephyrin clusters in approximately one-half of the injected γMNs parallels Ellaway and Murphy's (1981) findings of recurrent inhibition in 54% of recorded γMNs, compared to 91% of αMNs. Appelberg et al. (1983a–d) also suggested large variability in the amount of segmental afferent inhibitory influences received by γMNs, depending on their functional characteristics (extensor vs. flexors and static vs. dynamic). It is also interesting that the existence of size and complexity somatodendritic gradients in cluster architecture was independent of the density of gephyrin immunoreactivity expression in different neurons.

In conclusion, we have revealed that gephyrin localization and clustering vary significantly between different spinal cord neurons and that these patterns are meaningful in the context of the proposed functional roles of glycinergic inhibition over each class of neuron. Superimposed on the neuron-specific expression patterns, most spinal neurons exhibit somatodendritic gradients in the size and complexity of gephyrin-IR aggregates that might compensate for the electrotonic attenuation of synaptic events occurring in distal dendrites. The results suggest that molecular mechanisms that regulate glycine receptor clustering through the formation and shaping of gephyrin-IR clusters must do so in the context of the postsynaptic neuron identity and the location of the synapse on the dendritic tree.

ACKNOWLEDGMENTS

We are indebted to Dr. Bruce Walmsley for his comments on the manuscript and to Drs. H. Betz and J. Kirsch for the gift of antibody 2b. We thank Joel Chaney for his assistance with the statistical analysis. This work was supported by NIH-NINDS grants NS25547 (R.E.W.F.) and NS33555 (F.J.A.).

LITERATURE CITED

Alvarez, F.J., D.A. Harrington, D.E. Dewey, and R.E.W. Fyffe (1993) Distribution of glycine receptors on single intracellularly labeled motoneurons of the cat lumbar spinal cord. Soc. Neurosci. Abstr. *19:*193.

Appelberg, B., M. Hulliger, H. Johansson, and P. Sojka (1983a) Actions on gamma-motoneurones elicited by electrical stimulation of group I muscle afferent fibers in the hind limb of the cat. J. Physiol. (London) *335:*237–253.

Appelberg, B., M. Hulliger, H. Johansson, and P. Sojka (1983b) Actions on gamma-motoneurones elicited by electrical stimulation of group II muscle afferent fibres in the hind limb of the cat. J. Physiol. (London) *335:*255–273.

Appelberg, B., M. Hulliger, H. Johansson, and P. Sojka (1983c) Actions on gamma-motoneurones elicited by electrical stimulation of group III muscle afferent fibres in the hind limb of the cat. J. Physiol. (London) *335:*275–292.

Appelberg, B., M. Hulliger, H. Johansson, and P. Sojka (1983d) Recurrent actions on γ motoneurons mediated via large and small ventral root fibres in the cat. J. Physiol. (London) *335:*293–305.

Baldissera, F., H. Hultborn, and M. Illert (1981) Integration in spinal neuronal systems. In V.B. Brooks (ed): Handbook of Physiology: The Nervous System II. Motor Control, Part 1. Bethesda, MD: American Physiological Society, pp. 509–595.

Bekkers, J.M. (1994) Quantal analysis of synaptic transmission in the central nervous system. Curr. Opin. Neurobiol. *4:*360–365.

Betz, H. (1992) Structure and function of inhibitory glycine receptors. Q. Rev. Biophys. *25:*381–394.

Burke, R.E., L. Fedma, and A. Lundberg (1971) Spatial synaptic distribution of recurrent and group Ia inhibitory systems in cat spinal motoneurons. J. Physiol. (London) *214:*305–326.

Calverley, R.K., and D.G. Jones (1990) Contributions of dendritic spines and perforated synapses to synaptic plasticity. Brain Res. Rev. *15:*215–249.

Curtis, D.R., L. Hosli, and G.A.R. Johnston (1968) A pharmacological study of the depression of spinal neurons by glycine and related aminoacids. Exp. Brain Res. *6:*1–18.

Destombes, J., G. Horcholle-Bossavit, and D. Thiesson (1992) Distribution of glycinergic terminals on lumbar motoneurons of the adult cat: An ultrastructural study. Brain Res. *599:*353–360.

Eccles, J.C., P. Fatt, and K. Koketsu (1954) Cholinergic and inhibitory synapses in a pathway from motor axon collaterals to motoneurons. J. Physiol. (London) *126:*524–562.

Eccles, J.C., P. Fatt, and S. Landgren (1956) Central pathway for direct inhibitory action of impulses in largest afferent nerve fibres to muscle. J. Neurophysiol. *19:*75–98.

Edwards, F.A. (1995) LTP—A structural model to explain the inconsistencies. Trends Neurosci. *18:*250–255.

Ellaway, P.H., and P.R. Murphy (1981) A comparison of recurrent inhibition of alpha- and gamma-motoneurones in the cat. J. Physiol. (London) *315:*43–58.

Fyffe, R.E.W. (1991a) Spatial distribution of recurrent inhibitory synapses on spinal motoneurons in the cat. J. Neurophysiol. *65:*1134–1149.

Fyffe, R.E.W. (1991b) Glycine-like immunoreactivity in synaptic boutons of identified inhibitory interneurons in the mammalian spinal cord. Brain Res. *547:*175–179.

Fyffe, R.E.W., F.J. Alvarez, and D.A. Harrington (1993) Differential distribution of glycine receptors on interneurons in the cat spinal cord. Soc. Neurosci. Abstr. *19:*193.

Fyffe, R.E.W., F.J. Alvarez, D.A. Harrington, and D.E. Dewey (1995) Expression of glycine receptors in identified alpha and gamma motoneurons. In A. Taylor, M. Gladden and R. Durbaba (eds): Alpha and Gamma Motor Systems. New York: Plenum Press, pp. 421–428.

Holmes, W.R. (1995) Modeling the effect of glutamate diffusion and uptake on NMDA and non-NMDA receptor saturation. Biophys. J. *69:*1734–1747.

Hultborn, H., E. Jankowska, and S. Lindström (1971) Recurrent inhibition of interneurones monosynaptically activated from group Ia afferents. J. Physiol. (London) *215:*613–636.

Hultborn, H, S. Lindström, and H. Wigström (1979) On the function of recurrent inhibition in the spinal cord. Exp. Brain. Res. *37:*399–403.

Jankowska, E. (1992) Interneuronal relay in spinal pathways from proprioceptors. Progr. Neurobiol. *38:*335–378.

Kirsch, J., and H. Betz (1993) Widespread expression of gephyrin, a putative glycine receptor-tubulin linker protein, in rat brain. Brain Res. *621:*301–310.

Kirsch, J., and H. Betz (1995) The postsynaptic localization of the glycine receptor-associated protein gephyrin is regulated by the cytoskeleton. J. Neurosci. *15:*4148–4156.

Kirsch, J., D. Langosch, P. Prior, U.Z. Littauer, B. Schmitt, and H. Betz (1991) The 93-kDa glycine-receptor-associated protein binds to tubulin. J. Biol. Chem. *266:*22242–22245.

Kirsch, J., I. Wolters, A. Triller, and H. Betz (1993) Gephyrin antisense oligonucleotides prevent glycine receptor clustering in spinal neurons. Nature *266:*745–748.

Korn, H., and D.S. Faber (1991) Quantal analysis and synaptic efficacy. Trends Neurosci. *14:*442–448.

Koulen, P., M. Sassoe-Pognetto, U. Grünert and H. Wässle (1996) Selective clustering of GABAA and glycine receptors in the mammalian retina. J. Neurosci. *16:*2127–2140.

Larsson, L.-I. (1988) Immunocytochemistry: Theory and Practice. Boca Raton, FL: CRC Press.

Lisman, J.E., and K.M. Harris (1993) Quantal analysis and synaptic anatomy—Integrating two views of hippocampal plasticity. Trends Neurosci. *16:*141–147.

Mazzocchio, R., A. Rossi, and J.C. Rothwell (1994) Depression of Renshaw recurrent inhibition by activation of corticospinal fibres in human upper and lower limb. J. Physiol. (London) *481:*487–498.

Meyer, G., J. Kirsch, H. Betz, and D. Langosch (1995) Identification of a gephyrin-binding motif on the glycine receptor β subunit. Neuron *15:*563–572.

Moschovakis A.K., R.E. Burke, and R.E.W. Fyffe (1991) The size and dendritic structure of HRP-labeled gamma motoneurons in the cat spinal cord. J. Comp. Neurol. *311:*531–545.

Nicoll, M.J., and B. Walmsley (1991) A serial section electron microscope study of an identified Ia afferent collateral in the cat spinal cord. J. Comp. Neurol. *314:*257–277.

Pfeiffer, F., D. Graham, and H. Betz (1982) Purification by affinity chromatography of the glycine receptor of rat spinal cord. J. Biol. Chem. *257:*9389–9393.

Pfeiffer, F., R. Simler, G. Grenninlogh, and H. Betz (1984) Monoclonal antibodies and peptide mapping reveal structural similarities between the subunits of the glycine receptor of rat spinal cord. Proc. Natl. Acad. Sci. USA *81:*7224–7227

Pierce, J.P., and L.M. Mendell (1993) Quantitative ultrastructure of Ia boutons in the ventral horn: Scaling and positional relationships. J. Neurosci. *13:*4748–4763.

Rall, W., R.E. Burke, W.R. Holmes, J.J. Jack, S.J. Redman, and I. Segev (1992) Matching dendritic neuron models to experimental data. Physiol. Rev. *72:*S159–S186.

Redman, S. (1990) Quantal analysis of synaptic potentials in neurons of the central nervous system. Physiol. Rev. *70:*165–198.

Renshaw, B. (1941) Influence of discharge of motoneurons upon excitation of neighboring motoneurons. J. Neurophysiol. *4:*167–183.

Ross, H.-G., S. Cleveland, and J. Haase (1976) Quantitative relation between discharge frequencies of a Renshaw cell and an intracellularly depolarized neuron. Neurosci. Lett. *1:*105–108.

Ryall, R.W. (1970) Renshaw cell mediated inhibition of Renshaw cells: Patterns of excitation and inhibition from impulses in motor axon collaterals. J. Neurophysiol. *33:*257–270.

Schmitt, B., P. Knaus, C.-M. Becker, and H. Betz (1987) The Mr 93,000 polypeptide of the postsynaptic glycine receptor is a peripheral protein. Biochemistry *26:*805–811.

Schneider, S.P. and R.E.W. Fyffe (1992) Involvement of GABA and glycine in recurrent inhibition of spinal motoneurons. J. Neurophysiol. *68:*397–405.

Schröeder, S., W. Hoch, C.-M. Becker, G. Grenningloh, and H. Betz (1991) Mapping of antigenic epitopes on the α1 subunit of the inhibitory glycine receptor. Biochemistry *30:*42–47.

Spruston, N., D.B. Jaffe, and D. Johnston (1994) Dendritic attenuation of synaptic potentials and currents: The role of passive membrane properties. Trends Neurosci. *17:*161–166.

Takagi, T., I. Pribilla, J. Kirsch, and H. Betz (1992) Coexpression of the receptor-associated protein gephyrin changes the ligand binding affinities of α2 glycine receptors. FEBS Lett. *303:*178–180.

Todd, A.J., and A.C. Sullivan (1990) Light microscope study of the coexistence of GABA-like and glycine like immunoreactivities in the spinal cord of the rat. J. Comp. Neurol. *296:*496–505.

Todd, A.J., R.C. Spike, D. Chong, and M. Neilson (1995) The relationship between glycine and gephyrin in synapses of the rat spinal cord. Eur. J. Neurosci. *7:*1–11.

Tong, G., and C.E. Jahr (1994) Multivesicular release from excitatory synapses of cultured hippocampal neurons. Neuron *12:*51–59.

Tramu, G., A. Pillez, and J. Leonardelli (1978) An efficient method of antibody elution for the successive or simultaneous localization of two antigens by immunocytochemistry. J. Histochem. Cytochem. *26:*322–327.

Triller, A., F. Cluzeaud, P. Pfeiffer, H. Betz, and H. Korn (1985) Distribution of glycine receptors at central synapses: An immunoelectron microscopy study. J. Cell Biol. *101:*683–688.

Triller, A., F. Cluzeaud, and H. Korn (1987) Gamma-aminobutyric acid-containing terminals can be apposed to glycine receptors at central synapses. J. Cell Biol. *104:*947–956.

Triller, A., T. Seitanidou, O. Franksson, and H. Korn (1990) Size and shape of glycine receptor clusters in a central neuron exhibit a somatodendritic gradient. New Biol. *2:*637–641.

Trussell, L.O, S. Zhang, and I.M. Raman (1993) Desensitization of AMPA receptors upon multiquantal neurotransmitter release. Neuron *10:*1185–1196.

Van Keulen, L.C.M. (1981) Autogenetic recurrent inhibition of individual spinal motoneurons in the cat. Neurosci. Lett. *21:*297–300.

Walmsley, B. (1993) Quantal analysis of synaptic transmission. In D.T. Willis (ed): Electrophysiology: A Practical Approach. Oxford, England: Oxford University Press, pp. 109–141.

Windhorst, U. (1990) Activation of Renshaw cells. Progr. Neurobiol. *35:*135–179.